batteries

MDPI

Perspective

Use of Water-In-Salt Concentrated Liquid Electrolytes in Electrochemical Energy Storage: State of the Art and Perspectives

Shahid Khalid [1], Nicolò Pianta [1], Piercarlo Mustarelli [1,2,*] and Riccardo Ruffo [1,2]

[1] Department of Materials Science, University of Milano Bicocca, 20126 Milan, Italy
[2] National Reference Center for Electrochemical Energy Storage (GISEL), Consorzio Interuniversitario Nazionale per la Scienza e Tecnologia dei Materiali (INSTM), 50121 Firenze, Italy
* Correspondence: piercarlo.mustarelli@unimib.com

Abstract: Batteries based on organic electrolytes have been raising safety concerns due to some associated fire/explosion accidents caused by the unusual combination of highly flammable organic electrolytes and high energy electrodes. Nonflammable aqueous batteries are a good alternative to the current energy storage systems. However, what makes aqueous batteries safe and viable turns out to be their main weakness, since water molecules are prone to decomposition because of a narrow electrochemical stability window (ESW). In this perspective we introduce aqueous batteries and then discuss the state-of-the-art of water-in-salt (WIS) electrolytes for aqueous energy storage systems. The main strategies to improve ESW are reviewed, including: (i) the use of fluorinated salts to make a solid electrolyte interphase (SEI); (ii) the use of cost-effective and highly soluble salts to reduce water activity through super concentration; and (iii) the use of hybrid electrolytes combining the advantages of both aqueous and non-aqueous phases. Then, we discuss different battery chemistries operated with different WIS electrolytes. Finally, we highlight the challenges and future technological perspectives for practical aqueous energy storage systems, including applications in stationary storage/grid, power backup, portable electronics, and automotive sectors.

Keywords: metal-ion batteries; supercaps; water-in-salt; electrolyte; aqueous battery

Citation: Khalid, S.; Pianta, N.; Mustarelli, P.; Ruffo, R. Use of Water-In-Salt Concentrated Liquid Electrolytes in Electrochemical Energy Storage: State of the Art and Perspectives. *Batteries* **2023**, *9*, 47. https://doi.org/10.3390/batteries9010047

Academic Editor: Hans-Georg Steinrück

Received: 2 December 2022
Revised: 31 December 2022
Accepted: 4 January 2023
Published: 7 January 2023

1. Introduction

Driven by a variety of needs such as the grid-scale deployment of intermitted renewable energy sources together with the electrification of transportation, the development of efficient electrochemical energy storage systems (EESS) has long been at the forefront of energy technologies. Much progress has been accomplished thus far; for instance, the 2019 Nobel Prize in Chemistry honored the development of Li-ion batteries (LIBs) [1–3]. The electrolyte, which is an essential component of electrochemical systems, is often the limiting factor directly affecting the performance of EESS. Supported liquid electrolytes are still used in EESS because solid electrolytes are yet unable to compete in terms of cost, electrochemical, thermal, and interfacial properties. Therefore, the study and improvement of liquid electrolytes is remaining an active research area [4,5]. Currently, non-aqueous electrolytes based on organic solvents, ionic liquids, or deep eutectic solvents are primarily used to attain high operating voltage in EESS due to their broad electrochemical stability windows (ESW). The extended ESW of organic solvent-based electrolytes over water is mainly due to: (i) the absence of acidic protons, (ii) to the formation of an ionically conductive passivation layer formed by the decomposition of part of the electrolyte, as in the case of carbonate-based solutions in LIBs. This passivation layer was named solid electrolyte interphase (SEI) by Peled in 1979 after its discovery in 1970 by Dey et al. by soaking a Li metal anode in propylene carbonate (PC) based electrolyte [6–9]. SEI forms on the surface of most anodes and some cathodes, where it is generally referred to as the cathode

electrolyte interphase, CEI. The SEI is a thin solid film that allows the conduction of ions but not electrons, thus preventing further decomposition of electrolyte species and enabling efficient cycling of a secondary battery. However, poor safety, high cost, sluggish diffusion, and environmental concerns related to the use of organic electrolytes continue to be the relevant challenges to overcome for a complete acceptance of the LIB technology [4,10,11].

To improve the safety of LIBs, the highly flammable organic electrolytes used in these devices must be replaced with non-flammable alternatives. In this scenario, water emerges as a natural alternative for being nontoxic, non-flammable, and having excellent dielectric and rheological properties. Nevertheless, the narrow ESW of aqueous electrolytes arising from the low thermodynamic stability of water (1.23 V) hampers their practical use in high energy EESS [12,13]. Traditionally, progress in liquid electrolytes focused more on lower salt concentrations because the ionic mobility decreases with increasing salt concentration. For each solvent class, a characteristic concentration range marks the limit of the maximum ionic conductivity, for example, about 2 and 10 mol kg^{-1} for carbonate- and water-based electrolytes, respectively. Nonetheless, there have been multiple examples of deviation from this traditional paradigm in recent years. The earlier attempts date back to 1985 when Dahn and McKinnon reported a saturated electrolyte based on $LiAsF_6$ in PC exhibiting unusual intercalation behavior toward the host that was not possible in ordinary 1 M counterparts. The initial attempts to breach the concentration restraint were made with polymer electrolytes employing room-temperature ionic liquids (RTILs) [14–16]. A more recent breakthrough is the emergence of highly concentrated aqueous electrolytes also known as water-in-salt (WIS) electrolytes. The term WIS was first introduced by Suo et al. [17] for the 21 mol kg^{-1} LiTFSI aqueous electrolyte expanding the ESW to as high as 3 V through a combination of interfacial, bulk, and interphase effects. Super concentrated electrolytes based on lithium perfluoroalkyl-sulfonyl-amide and other related salts have higher ESW compared to traditional aqueous EESS such as lead acid and nickel metal hydride batteries [11,17–19]. Molecular dynamic simulations indicated that upon positive polarization the bis(trifluoromethanesulfonyl)imide (TFSI) anions accumulate at the electrode interphase forming a water-depleted region that promotes the oxidative stability of these electrolytes. On the other hand, the cathodic stability of these electrolytes is due to the formation of a robust solid electrolyte interphase (SEI) by the decomposition of TFSI anions. Still, the cathodic limit (1.9 V vs. Li^+/Li) of the 21 mol kg^{-1} LiTFSI-based electrolyte is not low enough for a traditional LIB negative electrode, for instance, $Li_4Ti_5O_{12}$ which works at 1.5 V vs. Li^+/Li. Besides, organic electrolyte-based batteries still outperform those with WIS electrolytes in terms of both cost and energy. Numerous studies were done to extend the cathodic limit at moderate salt concentrations by introducing additives [18,20–22]. The ESW of WIS electrolytes made it possible to develop novel, typically intercalation-type aqueous rechargeable batteries with higher cell voltages, thus narrowing the voltage gap compared to devices based on organic electrolytes.

This perspective aims at summarizing the progress made so far in the WIS and related electrolytes. First, we discuss the state-of-the-art in aqueous electrolytes. Then we highlight the challenges in the use of aqueous electrolytes for energy storage applications and the approaches used to solve the challenges in aqueous batteries. Finally, we conclude by providing a critical outlook for bringing aqueous batteries into real-world applications.

2. Strategies to Improve ESW

The superior performance of batteries based on organic electrolytes stems from the formation of stable SEI on the graphite anode thus expanding the ESW of these electrolytes from 3 V up to 4.2 V [8]. However, it is very difficult to realize a stable SEI in ordinary aqueous salt-in-water electrolytes because the reduction potential of water is very high compared to the decomposition potential of SEI-forming species. Thus, water decomposition is thermodynamically favored producing gaseous products instead of the reduction of the salt species. However, increasing the salt concentration in aqueous electrolytes significantly alters the decomposition potentials of water thus paving the way to the possibility of the

formation of a robust SEI [23,24]. Figure 1A shows a significant increase in the number of publications from 2015 to 2022 related to WIS electrolytes. A graphical representation of the water solvation structure in ordinary salt-in-water and water-in-salt electrolytes is presented in Figure 1B. Comparison of ESW for different electrolyte systems and strategies adopted to enhance ESW are given in Figures 1C and 1D, respectively.

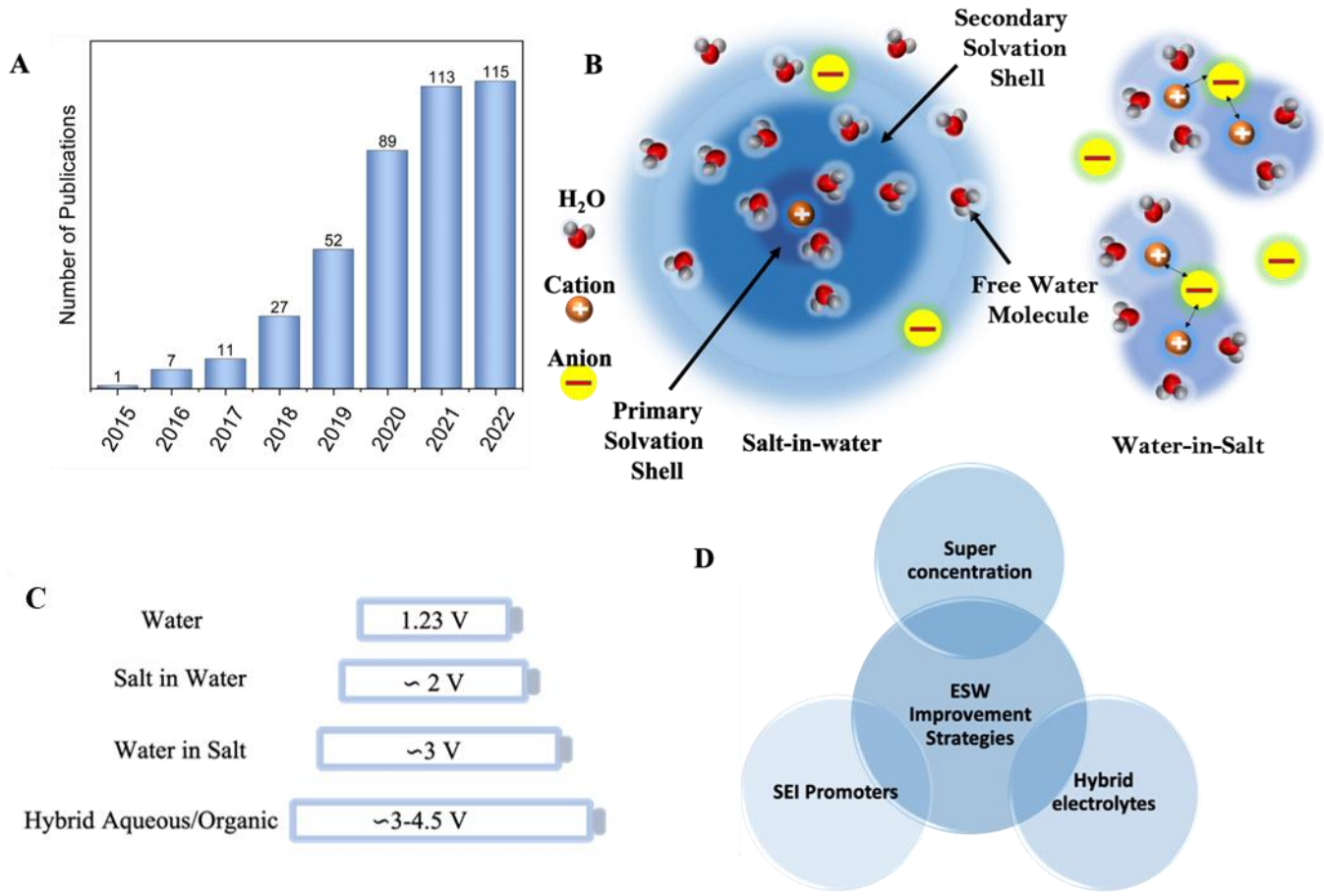

Figure 1. (**A**) Number of scientific publications related to WIS electrolytes (source Scopus); (**B**) Schematic illustration of lithium solvation shell in salt-in-water and WIS; (**C**,**D**) ESW expansion using different approaches.

2.1. ESW Expansion via SEI Promoters (TFSI, FSI, F-Based Systems)

The initial studies on explicit aqueous LIBs were reported by Dahn and co-workers in their 1994 publications employing a 5 M $LiNO_3$ aqueous electrolyte [25–27]. The cell constructed using 5 M $LiNO_3$ with 0.001 M LiOH employing VO_2 and $LiMn_2O_4$ showed a plateau at 1.5 V and delivered a practical specific energy of 55 Wh kg^{-1}. Around the same time that aqueous lithium-ion batteries had a research flameout in 2013, Lux et al. investigated the electrochemical stability of 2 M aqueous solutions of LiTFSI as a potential alternative to the $LiNO_3$ and $LiSO_2$ salt systems pioneered by Dahn and coworkers. The ionic conductivity of 2 M LiTFSI in water was found to be 41 mS cm^{-1} and its electrochemical stability window measured by Linear Sweep Voltammetry (LSV) was recorded to be 2.25 V, which was not apparently affected by a change in the pH. This was the first time that LiTFSI was used in aqueous Li-ion batteries. The work of Lux et al. unveiled the highly durable nature of TFSI anion at extreme pH and high temperatures (60 °C) thus making its way to the exotic field of aqueous electrolytes [28].

The research in aqueous electrolytes had an astonishing breakthrough in 2015 when Suo et al. [17] demonstrated that both the cathodic and anodic decomposition limits can be expanded by reducing water activity through manipulation of the Li-ion solvation

sheath. At dilute salt concentration (Figure 2A) i.e., less than 5 M, four water molecules in the primary solvation sheath of Li-ion exist, along with some loosely bonded water molecules in the secondary solvation shell. In such conditions, the dilute LiTFSI electrolyte can be regarded as a solvent-separated ion pair and is very much susceptible to hydrolysis beyond 2.63–3.86 V (vs. Li^+/Li). By increasing the concentration up to 21 mol kg^{-1} the number of water molecules per each Li^+ is reduced to 2.6 (Figures 1B and 2A) enabling the TFSI anion to form an intimate ion pair with the Li^+ ion as $Li_2(TFSI)(H_2O)_x$ leading to two consequences: (i) at very high concentration the electrochemical activity of water is significantly reduced due to the scarcity of free water molecules (strong resistance to oxidation on the cathode), and (ii) the coordination of Li^+ by multiple TFSI anions stabilizes the electron transfer during the reduction, thereby elevating the reduction potential for TFSI anions in the ion aggregate at the surface of the anode. According to DFT calculations, this contact ion pair is unstable to reduction below 2.9 V vs. Li^+/Li. Therefore, the TFSI anion in the $Li_2(TFSI)^+$ complex undergoes kinetic reduction (Figure 2B) before the reduction of water (2.63 V vs. Li^+/Li) forming a stable protective LiF-based layer on the surface of the anode. XPS analysis (Figure 2C) of the cycled anode confirmed the presence of a LiF-rich protective interphase on the anode formed from the reductive decomposition of the TFSI. Furthermore, to corroborate the preferential reduction of TFSI over H_2O, DFT analysis of density of states (DOS) showed that with increasing salt concentration the conduction band minimum of TFSI shifts to less cathodic potential, which causes a premature TFSI reduction forming a stable SEI layer and a delayed H_2O reduction (Figure 2D). Consequently, the onset potential for the hydrogen evolution reaction decreases to 1.9 V vs. Li^+/Li and the oxygen evolution potential is pushed to 4.9 V vs. Li^+/Li (Figure 2E) expanding the ESW up to 3 V [17,29].

Inspired by the extraordinary performance of LiTFSI, researchers started investigating other salts that could dissolve enough to satisfy the WIS condition. Becker et al. [30] demonstrated WIS electrolytes based on lithium (pentafluoroethanesulfonyl)-(trifluoromethanesulfonyl)imide LiPTFSI. A range of different electrolytes from 1 to 33 mol kg^{-1} was achieved. The 20 mol kg^{-1} electrolyte showed a good conductivity of 2.24 mS cm^{-1} at 25 °C. Other salts that can fulfil the WIS conditions include sodium bis(fluorosulfonylimide) (NaFSI) and lithium bis(fluorosulfonylimide) (LiFSI). Reber et al. studied the chemical stability of aqueous electrolytes prepared using LiFSI and NaFSI from a dilute concentration of 1 mol kg^{-1} to the highest possible concentration of 35 mol kg^{-1}. They monitored pH, optical appearance, and fluoride content of these electrolytes for a period of three months. No visual changes were observed for the electrolytes after four weeks at 30 °C, but for the 30 mol kg^{-1} and 35 mol kg^{-1} LiFSI-based electrolytes, which showed the formation of white precipitates (Figure 3A). Nonetheless, after three months changes in color and the presence of a large precipitate were observed. Other changes were the lowering of pH from the set value of 6 to less than 1 (Figure 3B) after storage for four weeks for the 35 mol kg^{-1} LiFSI, accompanied by the increase in fluoride content. In contrast, the pH of NaFSI solutions just slightly decreased to values between 5–4 (Figure 3C). These changes were more drastic at 60 °C (Figure 3D,E) and the formation of precipitate and color change was observed just after one week chiefly for the most concentrated (30 mol kg^{-1} and 35 mol kg^{-1}) LiFSI solutions. Interestingly, the NaFSI solutions showed no change in appearance, but the pH for the concentrated sample dropped to less than 1 (Figure 3F). The conductivity of the 20 mol kg^{-1} LiFSI/NaFSI solutions was found to be greater than 30 mS cm^{-1}. The conductivity values for 35 mol kg^{-1} LiFSI and NaFSI were found to be 11.2 mS cm^{-1} and 14.8 mS cm^{-1}, respectively, and both featured a stability window of 2.5 V at a cut-off current density of 5 μA cm^{-2} with Au electrodes [31].

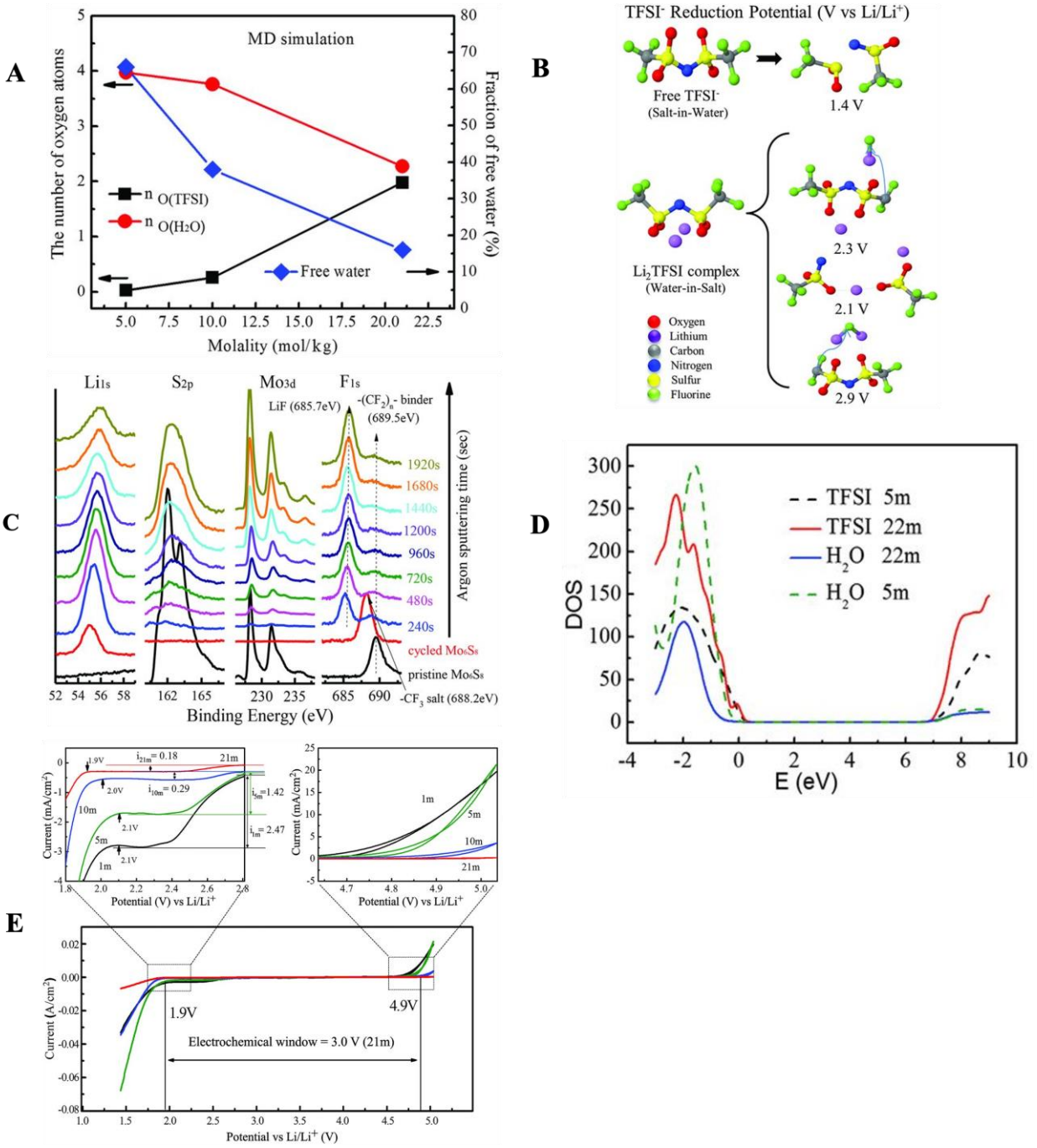

Figure 2. (**A**) No of O_2 atoms of H_2O and TFSI in the primary solvation shell (0.27 nm) of Li^+ and the fraction of free H_2O calculated through Molecular Dynamics Simulations; (**B**) predicted reduction potentials calculated via G4MP2 Quantum chemical calculations; (**C**) XPS spectra of pristine and cycled Mo_6S_8 anode; (**D**) "HSE06 DFT calculations" Projected DOS for LiTFSI-H_2O; (**E**) ESW measurement on stainless steel electrode by CV at 10 mVs^{-1}, 1 m (black), 5 m (green), 10 m (blue), 21 m (red). (**A**–**D**) are reprinted with permission from Ref. [17] Copyright 2015, AMERICAN ASSOCIATION FOR THE ADVANCEMENT OF SCIENCE.

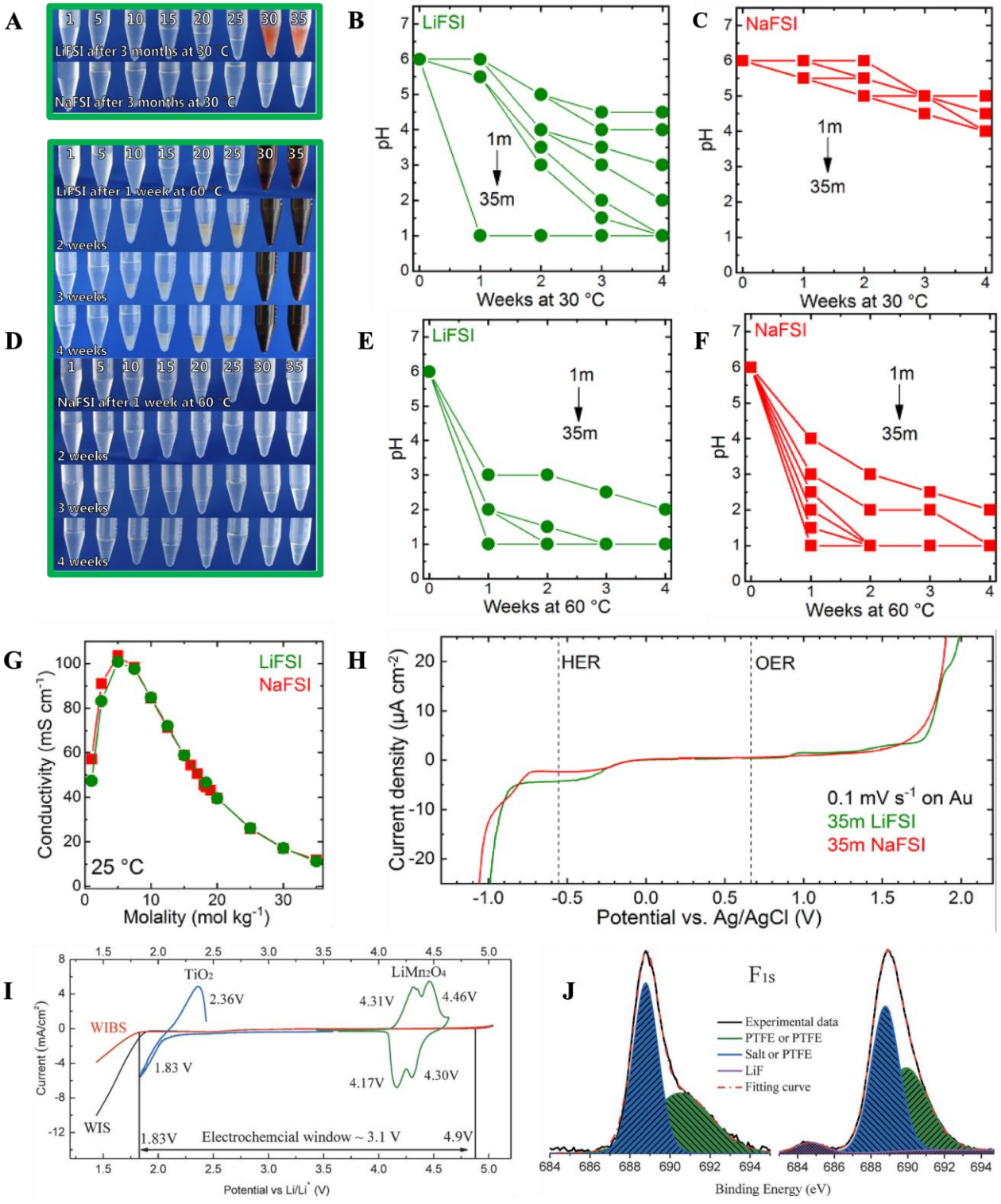

Figure 3. (**A**) photographs of LiFSI and NaFSI samples; (**B**,**C**) pH evolution of LiSFI/NaFSI as a function of time at 30 °C; (**D**) photographs of LiFSI and NaFSI samples at 60 °C; (**E**,**F**) pH evolution of LiSFI/NaFSI a function of time at 60 °C; (**G**) conductivity of LiFSI/NaFSI vs. concentration at 25 °C; (**H**) ESW of 35 mol kg^{-1} solution of LiFSI and NaFSI at 0.1 mV on Au electrodes; (**A**–**D**) are Reprinted with permission from Ref. [31] Copyright 2019, Elsevier B.V. (**I**) ESW of 28 molal water-in-(bi)salt (WIBS) electrolyte (21 mol kg^{-1} LiTFSI 7 mol kg^{-1} LiOTF); (**J**) XPS spectra showing the formation of LiF based SEI in the WIBS electrolyteand (**I**,**J**) are Reprinted with permission from Ref. [23], Copyright 2016, John Wiley & Sons, Inc.

In 2016 Suo et al. showed a hydrated salt that can be considered as a saturated electrolyte which is able to dissolve another similar anhydrous salt. With this idea in mind, they combined the 21 mol kg^{-1} LiTFSI (parent hydrate salt) with 7 mol kg^{-1} LiOTF (lithium triflate) and achieved a 28 mol kg^{-1} water-in-(bi)salt (WIBS) electrolyte with water to cation ratio of 2:1. This electrolyte enabled the formation of a more efficient SEI compared to 21 mol kg^{-1} LiTFSI (Figure 3J, XPS spectra) and showed an ESW of 3.1 V with cathodic and anodic limits at 1.83 V and 4.90 V vs. Li^+/Li as illustrated in Figure 3I [23].

2.2. ESW Expansion via Water Reduced Activity

Due to the high cost of the LiTFSI and related salts, Lukatskaya et al. demonstrated a WIBS electrolyte based on eco-friendly and highly cost-effective salts such as lithium-acetate (LiAc) and potassium acetate (KAc) [32]. Taking advantage of the high solubility of KAc (27 mol kg^{-1}) they prepared a range of electrolytes with different concentrations including the highly concentrated sample 32 mol kg^{-1} KAc 8 mol kg^{-1} LiAc which showed a conductivity of 5.3 mS cm^{-1} at 25 °C. The ESW of a series of acetate-based electrolytes is illustrated in Figure 4A,B.

Another highly concentrated aqueous electrolyte based on low-cost $NaClO_4$ 17 mol kg^{-1} was recently reported by Lee et al. and showed a stability window of 2.7 V vs. Na^+/Na having its cathodic and anodic limits at 2.7 V and 4.4 V, respectively, and exhibited a high conductivity of 108 mS cm^{-1} at 25 °C [33]. Similar to the binary cation-based WIBS (32 mol kg^{-1} KAc + 8 mol kg^{-1} LiAc) reported by Lukatskaya et al. for Li-ion batteries, a super concentrated mixed cation WIBS sodium electrolyte was reported by Han et al. [34]. This concentrated electrolyte (32 mol kg^{-1} KAc 8 mol kg^{-1} NaAc) showed an impressive ESW of 4.5 V (Figure 4C) making it possible to use standard Al current collectors.

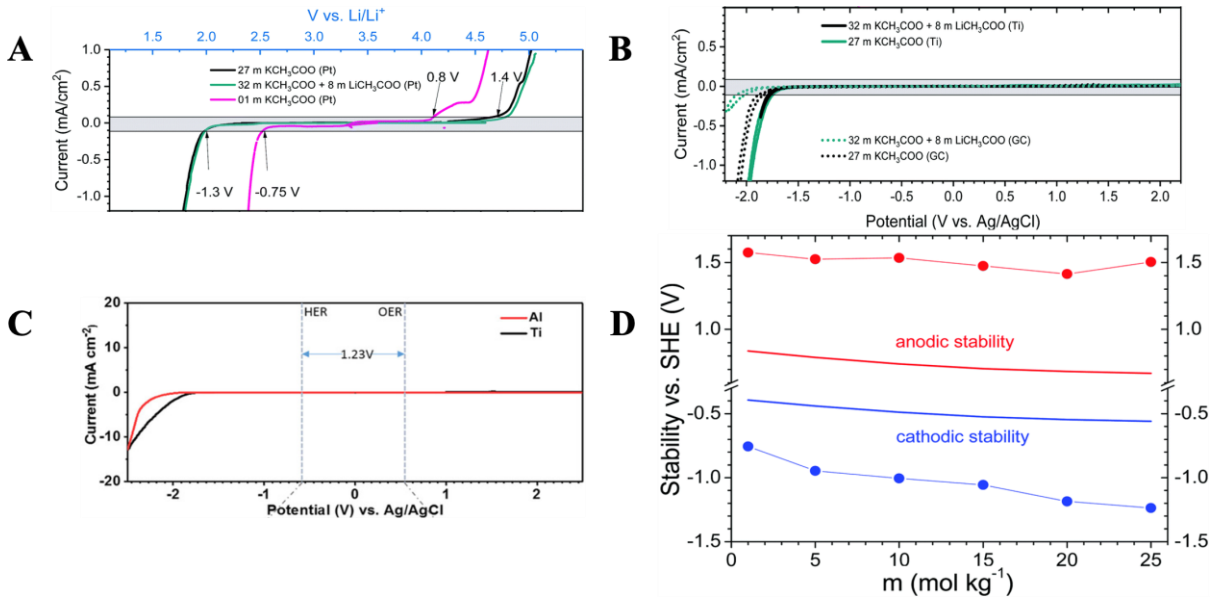

Figure 4. (**A**,**B**) LSV curves of a range of electrolytes based on lithium and potassium acetate; Reprinted with permission from Ref. [32], Copyright 2018, Royal Society of Chemistry (**C**) ESW of binary electrolytes of 32 m Kac + 8 m NaAc; Reprinted with permission from Ref. [34], Copyright 2018, Chemistry Europe (**D**) ESW data of a range of KAc solutions; Reprinted with permission from Ref. [35] Copyright 2021, Royal Society of Chemistry.

Recently, our group investigated the physical properties of a range of WIS electrolytes based on KAc from 1 mol kg^{-1} to 25 mol kg^{-1} (ESW presented in Figure 4D) [35]. We also investigated a binary electrolyte composed of 20 mol kg^{-1} KAc 7 mol kg^{-1} NaAc. The highest concentration stable at room temperature was the 20 mol kg^{-1} KAc 7 mol kg^{-1} NaAc having an improved ESW of 3.2 V [36].

2.3. ESW Expansion: The Hybrid Solvents Approach

Introducing a suitable organic component as a co-solvent to the WIS electrolyte is believed to further enhance the ESW by stabilizing the SEI. Using this approach, Wang et al. [37] prepared a novel aqueous/non-aqueous hybrid electrolyte by mixing the 21 mol kg^{-1} LiTFSI in water with a 9.2 mol kg^{-1} LiTFSI in the organic dimethyl carbonate (DMC) co-solvent. Due to the excellent solubility of LiTFSI in both water and DMC, the resulting hybrid electrolyte was highly homogenous and showed no phase separation. In this hybrid electrolyte, the aqueous component provided the advantage of non-flammability/safety while DMC further stabilized the SEI, thus pushing the cathodic limit as low as 1 V. According to MD simulation studies, the solvation structure of Li^+ was mainly dominated by $TFSI^-$, DMC, and water: on average Li^+ coordinated with two $TFSI^-$ with both the solvents (H_2O and DMC) in the first solvation shell. The resulted SEI was composed of both Li_2CoO_3 and LiF formed by the decomposition of Li_2TFSI^+ and Li_{2+}(DMC) complexes at 2.9 V and 1.5 V vs. Li^+/Li, respectively. The ESW reached 4.1 V (see Figure 5A).

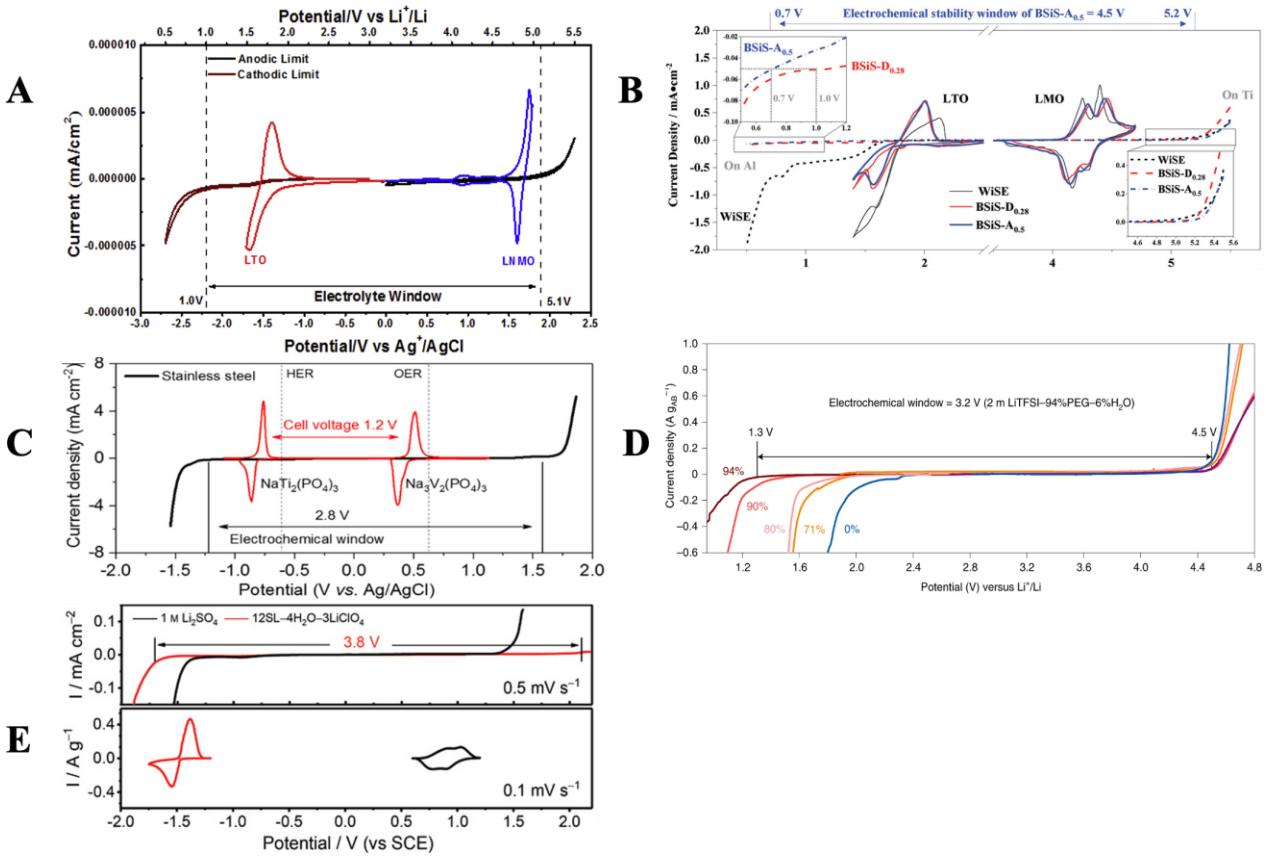

Figure 5. (**A**) CV of LTO and LNMO along with ESW in a DMC/LiTFSI/H_2O hybrid electrolyte; Reprinted with permission from Ref. [37], Copyright 2018, Elsevier B.V. (**B**) CV of LTO & LMO with ESW estimated in acetonitrile/LiTFSI/H_2O (BSiS-$A_{0.5}$) and DMC/LiTFSI/H_2O (BSiS-$D_{0.28}$) hybrid electrolytes; Reprinted with permission from Ref. [38], Copyright 2019, John Wiley & Sons, Inc. (**C**) ESW of hybrid electrolyte made with 7 m NaOTF in water + 8 m NaOTF in PC; Reprinted with permission from Ref. [39], Copyright 2018, American Chemical Society; (**D**) ESW of molecular crowding electrolytes composed of PEG/H_2O/LiTFSI; Reprinted with permission from Ref. [40], Copyright 2020, Springer Nature, LTd (**E**) CV of LTO/LMO and ESW estimation in hybrid sulfolane/H_2O/$LiClO_4$ electrolyte; Reprinted with permission from Ref. [41], Copyright 2022, John Wiley & Sons, Inc.

The addition of acetonitrile as co-solvent to the WIS electrolyte (15.2 mol kg^{-1} LiTFSI in water) was recently reported by Chen et al. [38] to promote the interphase chemistry

together with low-temperature operation due to the low freezing point (−48 °C) and low viscosity of acetonitrile. This hybrid electrolyte was in the liquid state even at a temperature as low as −20 °C where it exhibited a good conductivity value of 0.6 mS cm^{-1}. The addition of acetonitrile to the WIS electrolyte promoted the interactions of Li^+ with H_2O, thereby effectively decreasing the activity of free water and reducing the water population near the anode surface. The addition of acetonitrile improved SEI stability due to the formation of a uniform organic layer made of sulfamide and nitrile together with a LiF-rich inorganic layer. The ESW showed an expansion up to 4.5 V (see Figure 5B) for the acetonitrile-based electrolytes. The hybrid electrolyte approach was also explored for sodium-ion batteries, adding PC as a cosolvent along with water. The hybrid electrolyte comprising 7 mol kg^{-1} of NaOTF in water and 8 mol kg^{-1} NaOTF in PC in a weight ratio of 1:1 showed an ESW of 2.8 V (Figure 5C) [39].

A "molecular crowding" electrolyte composed of 2 M LiTFSI in 94% polyethylene glycol (PEG) and 6% water was reported by Xie et al. [40]. This hybrid electrolyte used the concept of restricting water molecules in the network of the crowding agent PEG through hydrogen bonds and expanded the ESW to 3.2 V (Figure 5D). Very recently, Liu et al. demonstrated the use of sulfolane as a cosolvent and antifreeze agent in an aqueous electrolyte, due to advantages such as high miscibility with water, low toxicity, high oxidation stability, and good coordination with water molecules. Using $LiClO_4$ as the salt, the hybrid electrolyte based on sulfolane and water showed a stability window of 3.8 V (Figure 5E). It was found that sulfolane could participate in the solvation shell of Li^+ and strengthen the OH bond of water. The $LiClO_4$ also acted as a fluxing agent by breaking the hydrogen bond network and preventing the aggregation and crystallization of the electrolyte, thereby resulting in a very low glass transition temperature of −110 °C [41]. Sulfolane was recently reported by Yuan and coworkers as a non-aqueous co-solvent to produce a hybrid (bi)solvent-in-salt (BSIS) electrolyte. This hybrid electrolyte offered a wide ESW at a significantly reduced salt concentration of 5.7 mol kg^{-1}. The enhanced ESW stems from the competitive coordination of sulfolane with water. The water molecules in the primary solvation shell were replaced by the electrochemically more stable molecules of sulfolane, which significantly decreased the hydrogen evolution [42]. Table 1 provides a list of various WIS electrolytes together with their ESW, ionic conductivities, voltage range, cost and NFPA 704 ratings.

Table 1. Physico-chemical and functional properties of some concentrated electrolytes.

							NFPA 704 Ratings *		
Electrolyte	**ESW (V)**	**Ionic Conductivity (mS cm^{-1})**	**Voltage Range vs. (Li^+/Li)**	**Current Collectors**	**Ref.**	**Cost ($ g^{-1})**	**Health**	**Instability/ Reactivity**	**Flammability**
21 m LiTFSI	3	10	1.9–4.9	Stainless Steel	[17]	3.5	*3*	*0*	1
35 m Lise	∼2.5	∼11.2	−2.4–4.97	Au	[31]	16.2	*3*	*0*	1
21 m LiTFSI + 7 m LiOTF	3.07	∼4.4	1.83–4.9	Stainless stee	[23]	3.3	3	0	1
32 m KOAc + 8 m LiOAc	2.7	5.3	1.97–4.7	Pt	[32]	0.32	2	1	1
32 m KAc + 8 m NaAc	>3	27	n.a.	Al/Ti	[34]	0.23	1	1	1
25 m NaFSI +10 m NaTFSI	2.7	11.8	n.a.	n.a.	[43]	68.2	3	0	1
LiTFSI/H_2O/$(ACN)_{3.5}$	3.26	13.2	n.a.	Stainless steel	[44]	0.92	3	0	0
21 m LiTFSI-H_2O/ 9.25 m LiTFSI in DMC (1:1)	4	3	1–5.1	Al/Ti	[37]	3.5	3	0	0
8 m $NaClO_4$/$(H_2O)_{1.5}$ $(ACN)_{2.4}$	3.16	42.1	1.81–4.95	Stainless steel	[45]	0.54	2	1	0

Table 1. *Cont.*

Electrolyte	ESW (V)	Ionic Conductivity (mS cm^{-1})	Voltage Range vs. (Li^+/Li)	Current Collectors	Ref.	Cost ($ g^{-1})	NFPA 704 Ratings *		
							Health	Instability/ Reactivity	Flammability
LiTFSI + 94%PEG + 6%H_2O	3.2	0.8	1.3–4.5	Coated Al	[40]	2.37	3	0	0
12SL–4H_2O–3$LiClO_4$	3.8	n.a.	1.68–5.08	Ti	[41]	0.64	3	2	1
SL:H_2O:LiTFSI (1.3:0.9:1)	5.1	0.8	1–5	Al/Ti	[42]	1.53	3	0	0
7 m NaOTF (H_2O) + 8 m NaOTF (PC)	2.8	~25	2.02–4.77		[39]	n.a.	1	1	0

* NFPA 704 standard offers a straightforward, quickly recognizable, and simple-to-understand system for identifying a material's specific risks. Ratings are from 0 to 3. Higher number indicates a higher risk.

3. Electrode Interfaces

3.1. Li-Intercalation Systems

The enhanced ESW of 3.0 V for the LiTFSI WIS electrolyte along with good ionic conductivity (10 mS cm^{-1} at 25 °C) enabled to couple several high energy cathode materials such as LiM_2O_4, $LiFePO_4$, $LiNi_{0.5}Mn_{1.5}O_4$, and low voltage anodes such as Mo_6S_8 and TiS_2 [17,46–48]. The LiTFSI WIS electrolyte was employed in $LiMn_2O_4/Mo_6S_8$ full-cell configuration which gave a specific energy of 78 W h kg^{-1} and cell voltage of 2.3 V for more than 1000 cycles. Figure 6A,B shows the galvanostatic cycling with potential limitation (GCPL) curves and the rate performance [17]. In a subsequent work by the same group the full cell based on $LiFePO_4/Mo_6S_8$ with 21 m LiTFSI as the electrolyte delivered a cell voltage of 1.5 V with a specific energy of 47 Wh kg^{-1} for over 1000 cycles with coulombic efficiency of 99%. The relatively lower cell voltage of 1.5 V was due to the moderate oxidation potential (3.5 V vs. Li^+/Li) of $LiFeO_4$ [46]. The 21 m LiTFSI WIS electrolyte was further explored by Sun et al. for $LiMn_2O_4/TiS_2$ based full cell which showed a cell voltage of 1.7 V with a high specific energy of 121 Wh kg^{-1} and a power density of 189 W kg^{-1} [49]. $LiNi_{0.5}Mn_{1.5}O_4$ is another well-studied high-voltage cathode with lithiation/delithiation plateaus between 4.6–4.8 V vs. Li^+/Li in organic electrolytes. Wang et al. found that the 21 m LiTFSI electrolyte caused a positive shift in the intercalation potentials (4.88 vs. 4.85 V and 4.96 vs. 4.90 V) for the $LiNi_{0.5}Mn_{1.5}O_4$ cathode due to the high salt concentration, pushing the second lithiation potential of 4.96 V beyond the anodic stability limit (4.9) of the electrolyte. This problem was solved by the addition of 0.1 vol% bis(trifluoromethane sulfonimide $(CF_3SO_2)_2NH$ to the 21 m LiTFSI electrolyte which enhanced the anodic stability limit to 5.0 V. The enhanced anodic limit allowed the $LiNi_{0.5}Mn_{1.5}O_4$ to charge up to 5.05 V achieving a high capacity of 125 m Ahg^{-1} [47]. The GCPL curves are shown in Figure 6C,D.

As a promising alternative to LMO, $LiCoO_2$ is a widely studied cathode in organic electrolytes. However, $LiCoO_2$ must be charged to a high cut-off potential to completely utilize its capacity at the expense of structural damage due to cobalt dissolution and severe side reactions with the electrolyte [50–52]. Tris(trimethylsilyl)borate (TMSB) as an electrolyte additive to the 21 m LITFSI WIS electrolyte was reported to be capable of stabilizing the cathode by the formation of cathode electrolyte interphase (CEI). TMSB increased ESW by oxidizing before water and TFSI anion, to produce orthosilicic acid and boric acid which deposited over the cathode surface forming the CEI. The CEI prevented further electrolyte decomposition and suppressed Co dissolution from the cathode. Operating at a high cell voltage of 2.5 V, CEI-protected $LiCoO_2$ coupled with Mo_6S_8 in a full cell configuration delivered a high specific energy of 120 Wh kg^{-1} [53,54]. Together with the standard WIS, WIBS electrolytes were also found to be promising candidates for aqueous Li-ion chemistries. The super-concentrated 28 mol kg^{-1} WIBS electrolyte composed of 21 mol kg^{-1} LiTFSI and 7 m mol kg^{-1} LiOTF enabled a 2.5 V full cell with $LiMn_2O/TiO_2$ delivering a high specific energy of 100 Wh kg^{-1}. The GCPL profile and rate performance for the $LiMn_2O/TiO_2$ couple are displayed in Figure 6E,F. Moreover, the WIBS based on

LiTSFI + LiOTF showed a liquidus temperature of 21.5 °C and a conductivity of 6.5 mS cm^{-1} at room temperature [23]. A hydrate melt electrolyte $Li(TFSI)_{0.7}(N(SO_2C_2F_5)_2)_{0.3}$ was reported by Yamada et al. to show good conductivity of 3 mS cm^{-1}, although it exhibited high viscosity of 203 mP at 30 °C, along with an enhanced anodic limit of 5.05 V vs. Li^+/Li. This novel electrolyte allowed the successful operation of low-voltage LTO in a couple with both LNMO and $LiCoO_2$ delivering a high specific energy >130 Wh kg^{-1} as reported in Figure 6G,H [55]. Benefiting from the low cost of acetate-based common salts such as Kac and LiAc, a highly concentrated 40 m WIBS electrolyte made of 32 mol kg^{-1} Kac and 8 mol kg^{-1} LiAc allowed a 2.5 V full cell based on LMO and C-TiO_2 to deliver a capacity of 45 mAh g^{-1} [32].

3.2. Other Intercalation Chemistries

The concept of WIS electrolytes can significantly broaden the battery chemistry. Apart from LIBs, these electrolytes can be used in other intercalation chemistries such as sodium and potassium ion batteries as well as in other metal-based EESS. Aqueous sodium-ion batteries are attracting the attention of the scientific community as an alternative to Li-ion batteries owing to the low cost and abundant presence of sodium in nature. A concentrated aqueous electrolyte based on 9.3 m NaOTF was first reported by Suo et al. to successfully form a stable Na-ion conducting SEI pushing the decomposition limit of water to 1.7 V (cathodic) and 4.2 V (anodic), respectively [56]. Theoretical investigation suggests that at a NaOTF concentration less than 5 mol kg^{-1} the solvation sheath of Na^+ ion at maximum contains two layers, with six tightly bonded H_2O molecules in the first shell, and another six loosely bound H_2O molecules in the second shell. However, when the concentration is increased above 9 mol kg^{-1} the presence of H_2O molecules in the primary solvation shell is significantly reduced and the electrolyte can be considered as a molten salt. In contrast to LiTFSI, where a very large concentration of 21 mol kg^{-1} is required to achieve a stable interphase, the NaOTF salt guarantees the formation of stable SEI at a relatively lower salt concentration of just 9.26 mol kg^{-1}. In fact, for this concentration 63% of the salt species exist as ion contact pairs which help increase the salt reduction potential above the water reduction potential. The ESW of the NaOTF-based aqueous electrolyte was found to be 2.5 V, allowing the successful operation of $NaTi_2(PO_4)_3/Na_{0.66}[Mn_{0.66}Ti_{0.34}]O_2$ full cell with excellent cycling behavior. The electrochemical performance of 9.26 mol kg^{-1} in comparison with 2 mol kg^{-1} NaTFSI and 1 mol kg^{-1} Na_2SO_4 is presented in Figure 7A. Another WIS electrolyte composed of low-cost $NaClO_4$ 17 mol kg^{-1} enabled a full cell based on $NaTi_2(PO_4)_3/Na_4Fe_3(PO_4)_2(P_2O_7)$ to deliver a capacity of 45 mAh g^{-1} at 0.2 C and 34 mAh g^{-1} at 10 C. The full cell showed good rate capability with a capacity retention of 75% after 200 cycles with a CE of 99% [33]. As an example of the mixed cation approach based on low-cost and eco-friendly acetate salts, super concentrated 32 mol kg^{-1} KAc + 8 mol kg^{-1} NaAc WIBS electrolyte allowed to couple two $Na_2VTi(PO_4)_3$ electrodes and the cell showed a capacity of 55 mA h g^{-1} [57]. Salt crystallization in highly concentrated electrolytes is a big challenge and has a direct effect on the cell life cycle. Reber et al. mixed salts with asymmetric anions, e.g., NaFSI and NaFTFSI. A WIBS electrolyte based on asymmetric anions 25 mol kg^{-1} NaFSI + 10 mol kg^{-1} NaFTFSI enabled a 2.0 V full cell based on $NaTi_{2(}PO_4)_3/Na_3(VPO_4)2F$ with a maximum capacity of 83 mAh g^{-1} (Figure 7B) in a temperature range of −10 °C to 30 °C. The cell operated at −10 °C for more than 500 cycles without any salt crystallization [43].

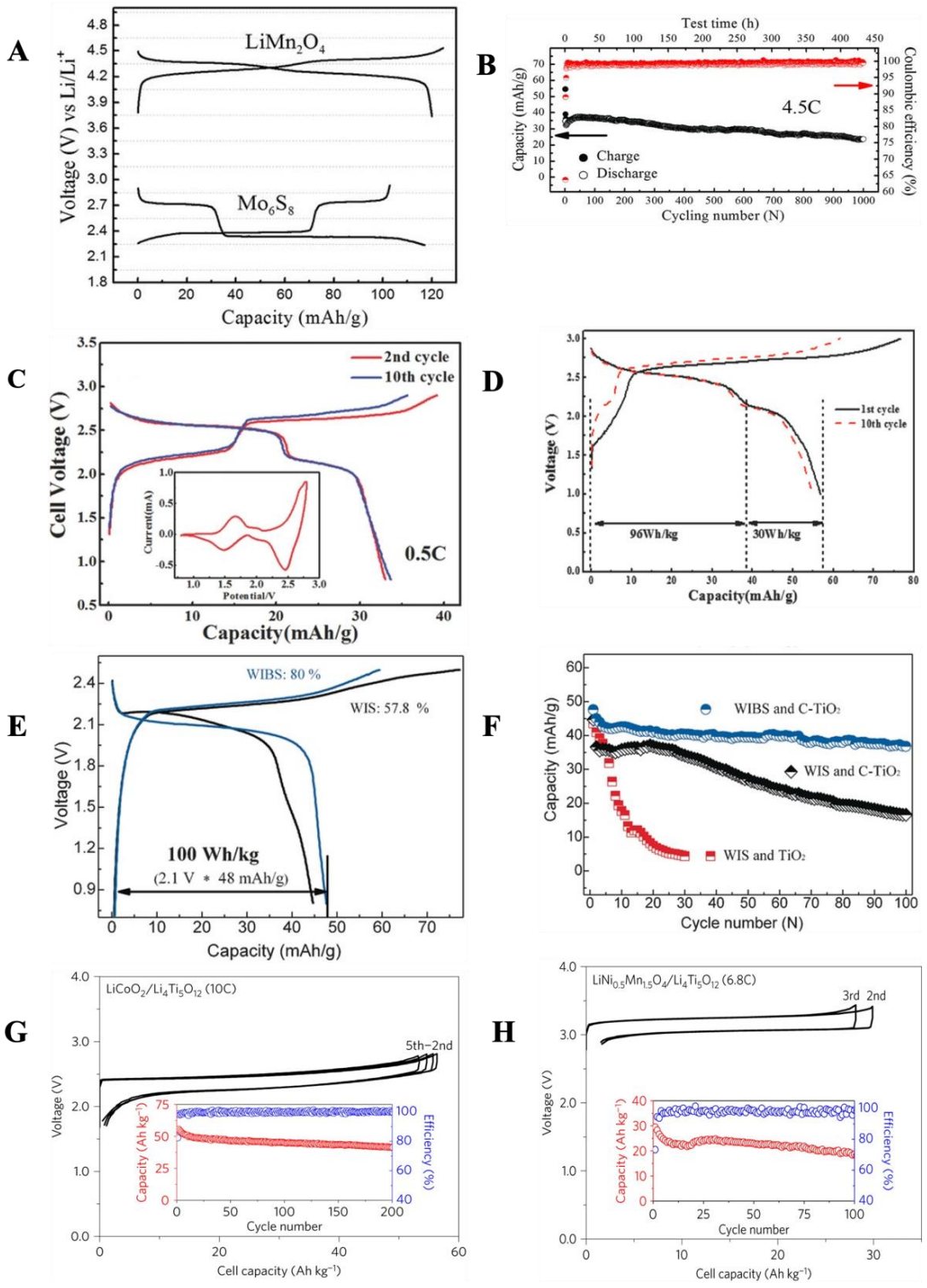

Figure 6. (**A**) GCPL curves $LiMn_2O_4/Mo_6S_8$; (**B**) Rate performance of $LiMn_2O_4/Mo_6S_8$ at 4.5 C; "Reprinted with permission from Ref. [17] Copyright 2015, Copyright 2015, AMERICAN ASSOCIATION FOR THE ADVANCEMENT OF SCIENCE (**C**) GCPL curves of $Mo_6S_8/LiNi_{0.5}Mn_{1.5}O_4$ before and (**D**) after pH adjustment; "Reprinted with permission from Ref. [47], Copyright 2016, John Wiley & Sons, Inc. (**E**) GCPL profile and (**F**) rate performance for the $LiMn_2O/TiO_2$ couple in the WIBS and standard 21 m LiTFSI; Reprinted with permission from Ref. [23], Copyright 2016, John Wiley & Sons, Inc. (**G**,**H**) electrochemical performance of LNMO/LTO and $LiCoO_2$/LTO full cells; Reprinted with permission from Ref. [55], Copyright 2016, Springer Nature, Ltd.

Rechargeable potassium ion batteries also gained significant attention owing to the abundant, low cost, and non-toxic nature of potassium. Additionally, the lower reduction potential (−2.91 V vs. SHE) accounts for high energy, while the small Stokes radius of solvated K^+ ions in the electrolyte can offer superior rate capability. The first WIS electrolyte (super-concentrated 30 mol kg^{-1} KAc) was reported by Leonard et al. [58]. The electrolyte had ESW of 3.2 V and enabled the reversible operation of $KTi_2(PO_4)_3$ as the anode with specific capacity of 53 mAh g^{-1}. Long cycling at 1 A g^{-1} (See Figure 7C) revealed a capacity fade from 53 to 35 mAh g^{-1} during the initial 500 cycles, a stabilization at 30 mAh g^{-1} for the next 5500 cycles, and a further increase for the next 5000 cycles stabilizing at 40 mAh g^{-1} after 11,000 cycles with an overall capacity retention of 69%. Jiang et al. [59] reported a highly concentrated WIS electrolyte employing 22 mol kg^{-1} KCF_3SO_3. Using this WIS electrolyte, a full cell was fabricated with a Mn-rich KFeMnHCF cathode and a 3,4,9,10-perylenetetracarboxylic diimide (PTCDI) organic anode. Operating above 2 V, the full cell achieved superior performance with a high capacity of 135 mAh g^{-1} and an excellent rate capability (showing capacity retention of 70% at 100 C), along with outstanding cycling stability (90% of capacity retention after 2000 cycles). Figure 7D demonstrates the long cycling performance at 4 C for the KFeMnHCF/PTCDI/22 M KCF_3SO_3 coin-type full cell. The electrolyte exhibited good ionic conductivity of 76 mS cm^{-1} at room temperature and 10 mS cm^{-1} at −20 °C thus enabling operation in the temperature range from –20 °C to 60 °C. Recently, Liu et al. reported a super concentrated 40 mol kg^{-1} potassium formate (CHOOK) based WIS electrolyte where the H_2O:salt ratio was as low as 1.3:1 [60]. This electrolyte showed a wide ESW of 4 V measured using glassy carbon as current collector. Taking advantage of the high solubility of potassium bis(fluorosulfonyl)imide (KFSI), Chen et al. reported a 30 mol kg^{-1} KFSI WIS electrolyte. This highly concentrated electrolyte showed a wide ESW of 3.97 V and allowed the successful operation of β-perylene-3,4,9,10-tetracarboxylic dianhydride (β-PTCDA) anode suppressing the H_2 evolution. Moreover, the high salt concentration effectively solved the problem of material dissolution and decreased the charge transfer resistance, so improving the kinetics. The β-PTCDA achieved a reversible capacity of 109 mAh g^{-1} at a current density of 8 A g^{-1} and showed a life span of 500 cycles at a current density of 2 A g^{-1} [61]. The 22 mol kg^{-1} KCF_3SO_3 was further explored by Liang et al., using $K_{0.5}V_2O_5$ as a cathode which delivered a high capacity of 116 mA h g^{-1} at 1 C and superior capacity retention of 65 mAh g^{-1} at 50 C. A full cell was fabricated using the KVO cathode and PTCDI anode which showed excellent capacity retention of 77.3% after 20,000 cycles at 10 C [62].

3.3. Metallic Batteries

Batteries based on polyvalent metal ions can offer higher volumetric energy density compared to monovalent metal ion batteries. In contrast, the high charge density of multivalent cations hinders the diffusion process due to stronger Coulombic cation-anion interactions. Interestingly, the charge density of a multivalent cation is reduced in an aqueous electrolyte due to the shielding effect of H_2O molecules which improves the diffusion kinetics [63].

Aqueous zinc-ion batteries attracted great attention in recent years due to Zn high theoretical capacity, low cost, high abundance, and low toxicity. Unlike other metal ion chemistries where a stable SEI is crucial for proper operation, metallic zinc exhibits good electrochemical stability in aqueous media due to its relatively higher reduction potential of −0.76 vs. SHE. Indeed, irreversible Zn plating/stripping at the anode surface and the dissolution of the most available cathode materials (Prussian blue analogs and manganese or vanadium-based oxides) are the main problems to be solved. At low salt concentration in aqueous electrolytes, the Zn^{2+} is strongly coordinated by six water molecules and can be viewed as a $Zn(H_2O)_6^{2+}$ cation. In such dilute systems, the performance is significantly restricted by the severe irreversibility of Zn plating/stripping because of the high energy barrier for the solvated Zn^{2+}. Besides, OH^- ions from water degradation can form $Zn(OH)_2$ and ZnO on the anode surface, accelerating the dendrite formation and electrolyte draining.

Therefore, a highly reversible Zn-anode requires two things to be worked out: (i) to limit the electrochemical activity of free H_2O molecules, and (ii) to modify the solvation structure to facilitate the energetically favorable Zn plating/stripping [64]. Wang et al. reported a 21 mol kg^{-1} WIBS electrolyte composed of 20 mol kg^{-1} LiTFSI 1 mol kg^{-1} $Zn(TFSI)_2$ [65]. MD simulations and structural and spectroscopic studies revealed that at higher $TFSI^-$ concentrations the Zn^{2+} solvation structure is greatly altered from $Zn(H_2O)_6$ by ion pairs interaction, and the Zn^{2+} solvation shell is mainly occupied by TFSI anions. This modification of the primary solvation shell enabled the Zn plating/stripping without dendrite formation with a high Coulombic Efficiency (CE) of 100% in a symmetric Zn||Zn cell. This WIBS electrolyte was also employed in a hybrid cell based on $LiMn_2O_4$ and Zn anode, which showed good reversible Li intercalation behavior for LMO and reversible Zn plating/stripping for Zn anode. The hybrid Zn/LMO full cell achieved a high specific energy of 70 Wh kg^{-1} and excellent cycling performance [65] (See Figure 7E) with 85% capacity retention after 4000 cycles with a CE of 99.9%. Another super-concentrated electrolyte composed of 21 mol kg^{-1} LiTFSI 1 mol kg^{-1} $Zn(CF_3SO_3)_2$ was reported by Hu et al. and employed in a full cell based on V_2O_5 cathode and Zn anode. The high salt concentration ensured the reversible operation of Zn anode and the presence of both Li^+ and Zn^{2+} resulted in co-intercalation of Li^+/Zn^{2+} in the V_2O_5 achieving a high capacity of 238 mAh g^{-1} at 50 mA g^{-1} and 80% capacity retention after 2000 cycles [66] (See Figure 7F). Zhao et al. reported a WIBS electrolyte composed of 21 mol kg^{-1} LITFSI 0.5 mol kg^{-1} $ZnSO_4$ which allowed a $Zn/LiMn_{0.8}Fe_{0.2}PO_4$ hybrid cell to operate above 1.8 V achieving a high specific energy of 183 Wh kg^{-1} [67]. To overcome the issue of the high cost of the fluorinated salts, Zhang et al. reported a 30 m $ZnCl_2$ WIS electrolyte which showed an ESW of 2.3 V and enabled a Zn||Zn symmetric cell with 95.4% CE [68].

Other metallic battery chemistries based on Mg, Ca, and Al suffer the same issues of higher charge density which greatly restricts the diffusion, but it was found that by using concentrated aqueous electrolytes the shielding effect of H_2O molecules can play a beneficial role. A concentrated aqueous electrolyte made of 8.37 M $Ca(NO_3)_2$ was studied by Lee et al. for use in Ca ion batteries [69]. It was found that, compared to 1 M $Ca(NO_3)_2$, the concentrated electrolyte reduced the size of the hydrated cation due to the non-availability of free water for the formation of a secondary solvation shell. This reduction in the size of the hydrated cation resulted in improved diffusion inside the channel structure of the Prussian blue analogs (PBAs), so increasing the capacity by 13%. The highly concentrated electrolyte showed good cyclic stability of PBA electrode with 97% capacity retention after 150 cycles, whereas the capacity retention in 1 M electrolyte was only 58%. Recently, Adil et al. [70] demonstrated a non-toxic, low cost, and non-corrosive WIS electrolyte based on $Ca(NO_3)_2$ which showed an ESW of 2.12 V for concentration 15–20 mol kg^{-1} compared to 1.15 V for dilute 1 mol kg^{-1}. Figure 7G demonstrates the electrochemical performance of a full cell fabricated with CaxCuHCF||PANI/CC using this WIS electrolyte, which delivered an excellent specific energy of 232 Wh kg^{-1} and power density of 69 W kg^{-1} along with good cycle life, retaining 80% capacity after 1800 cycles at 3 Ag^{-1} with 99.9% CE.

A novel Mg-based WIS electrolyte comprised of $MgCl_2 \cdot 6H_2O$:H_2O with a mass ratio of 25:1 was reported by Leong et al. showing an impressive ESW of 3.6 V. A full-cell configuration with a copper hexacyanoferrate cathode and Mg anode displayed a high voltage plateau at 2.4–2.0 V with a specific capacity of 47 mAh g^{-1} and CE of 99% for more than 700 cycles. The rate performance of the Mg metal anode/CuHCF cathode is displayed in Figure 7H [71].

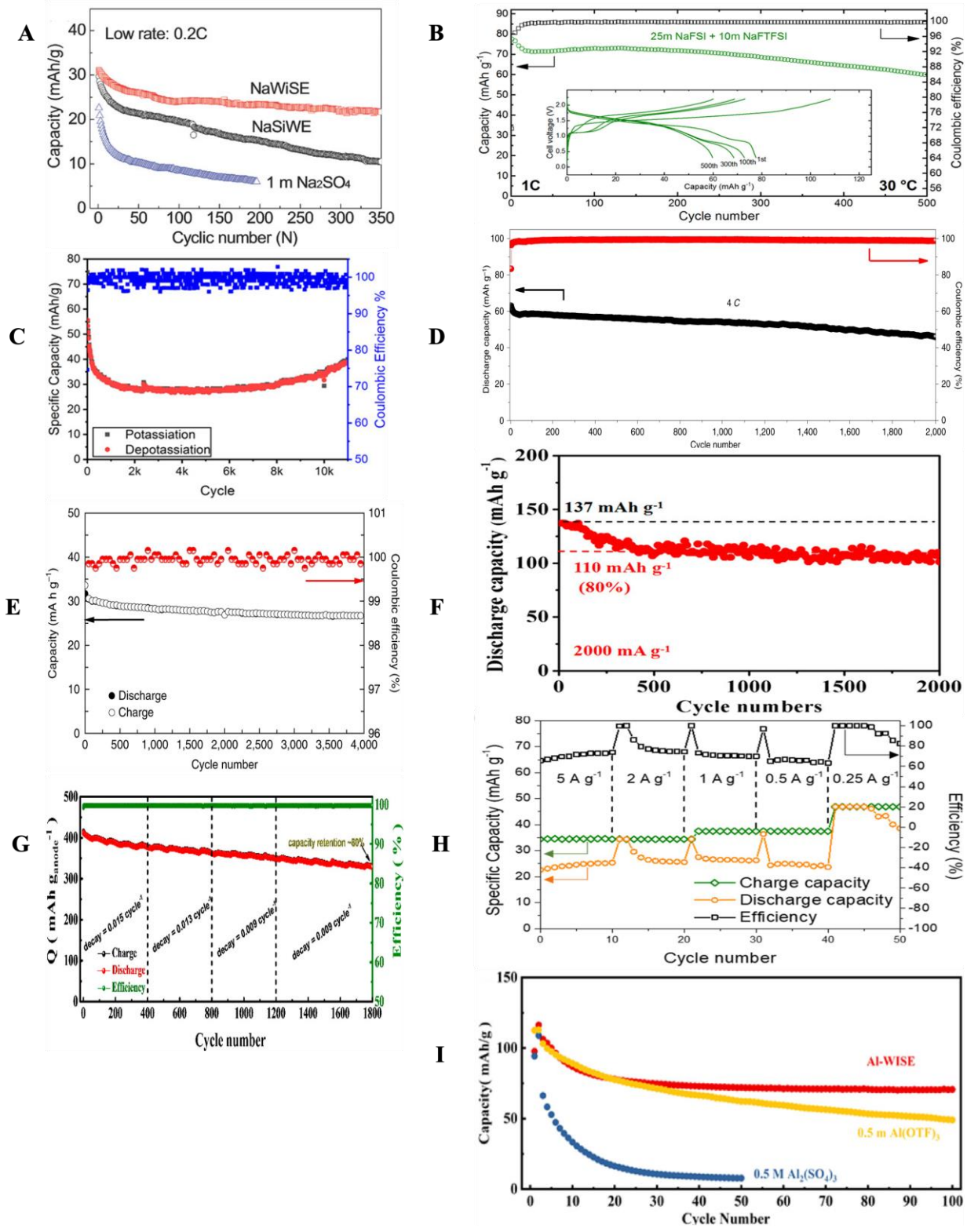

Figure 7. (**A**) The electrochemical performance of 9.26 mol kg^{-1} in comparison with 2 mol kg^{-1} NaTFSI and 1 m Na_2SO_4; [56] (**B**) GCPL profile and Rate performance of full cell based on $NaTi_2(PO_4)_3/Na_3(VOPO_4)_2F$, capacity in green and coulombic efficiency in black; Reprinted with permission from Ref. [43], Copyright 2019, American Chemical Society (**C**) Long cycling at 1 A g^{-1} for a $KTi_2(PO_4)_3$ anode in 30 m Kac; (**A**,**C**) are Reprinted with permission from Ref. [58], Copyright 2018, American Chemical Society (**D**) long cycling performance at 4 C for the KFeMnHCF/PTCDI/22 M KCF_3SO_3, capacity in black and coulombic efficiency in red; Reprinted with permission from Ref. [59],

Copyright 2019, Springer Nature, Ltd. (**E**) Zn/LMO full cell long cycling; Reprinted with permission from Ref. [65], Copyright 2018, Springer Nature, Ltd. (**F**) rate performance of Zn/V_2O_5; Reprinted with permission from Ref. [66], Copyright 2017, American Chemical Society (**G**) electrochemical performance of a full cell fabricated with CaxCuHCF||PANI/CC in WIS electrolyte; Reprinted with permission from Ref. [70], Copyright 2022, American Chemical Society (**H**) rate performance of the Mg metal anode/CuHCF cathode; Reprinted with permission from Ref. [71], Copyright 2022, American Chemical Society (**I**) cycling performance and coulombic efficiency of the PBA cathode in mol kg^{-1} $Al(CF_3SO_3)_2$ WIS electrolyte and in 0.5 mol kg^{-1} $Al_2(SO_4)_3$ and 0.5 mol kg^{-1} $Al(OTF)_3$; Reprinted with permission from Ref. [72], Copyright 2019, American Chemical Society.

Al-ion batteries offer the highest theoretical capacity of 2980 mAh g^{-1} (8046 mAh cm^{-3}) among all the rechargeable metal ion systems, but the technology greatly suffers of the issue of nonavailability of suitable electrolytes to allow reversible Al plating/stripping at the anode. Moreover, the low reduction potential (−1.68V vs. SHE) of the Al^{3+} also prevents the cell from functioning properly in aqueous media due to the unavoidable Hydrogen Evolution Reaction (HER) at the anode at such a low potential. Zhou et al. [72] recently showed that replacing the ordinary dilute aqueous electrolyte with a 5 mol kg^{-1} $Al(CF_3SO_3)_2$ WIS electrolyte can widen the ESW to support the reversible Al plating/stripping on the anode. At dilute salt concentration of 1 mol kg^{-1} $Al(CF_3SO_3)_2$ the solvation structure of the Al^{3+} is made by six H_2O molecules arranged both in the primary and secondary solvation sheath of the cation. However, when the concentration is increased to 5 mol kg^{-1} the solvation structure is greatly modified and ∼28% of the species exist as intimate-ion-pairs which can be viewed as $[(Al^{3+})_x–(CF_3SO_3{}^-)_y–(H_2O)_m]$, 7% of the species exist as loose contact ion-pairs as $[Al^{3+}(H_2O)_n–(CF_3SO_3{}^-)_3]$, and the population of free anion as $[(CF_3SO_3{}^-)_z–(H_2O)_w]$ is about 0%. This modification of the solvation structure extended the ESW to 2.65 V which enabled a full cell by coupling Al anode and a $(K_{0.2}Fe[Fe(CN)_6]_{0.79}\cdot 2.1H_2O)$ PBA cathode achieving an initial cycle capacity of 116 mA h g^{-1}. The cycling performance and CE of the PBA cathode in 5 mol kg^{-1} $Al(CF_3SO_3)_2$ WIS electrolyte and in 0.5 mol kg^{-1} $Al_2(SO_4)_3$ and 0.5 mol kg^{-1} $Al(OTF)_3$ for comparison is shown in Figure 7I.

3.4. Supercaps

Apart from secondary ion batteries, the WIS electrolytes are also used in supercapacitors, and the devices showed much higher cell voltages compared to ordinary dilute electrolytes together with the advantages of high-power density and safety of aqueous electrolytes. Apart from symmetric devices, asymmetric supercapacitors were also fabricated using WIS electrolytes. A good example is a hybrid supercapacitor demonstrated by Zhang et al. including a well-protected Li anode coupled with a pseudocapacitive MnO_2 cathode, which delivered a high cell voltage of 4.4 V, a specific energy of 405 Wh kg^{-1}, and a power density of 0.88 kW kg^{-1}. The galvanostatic charge–discharge curves are reported in Figure 8A [73].

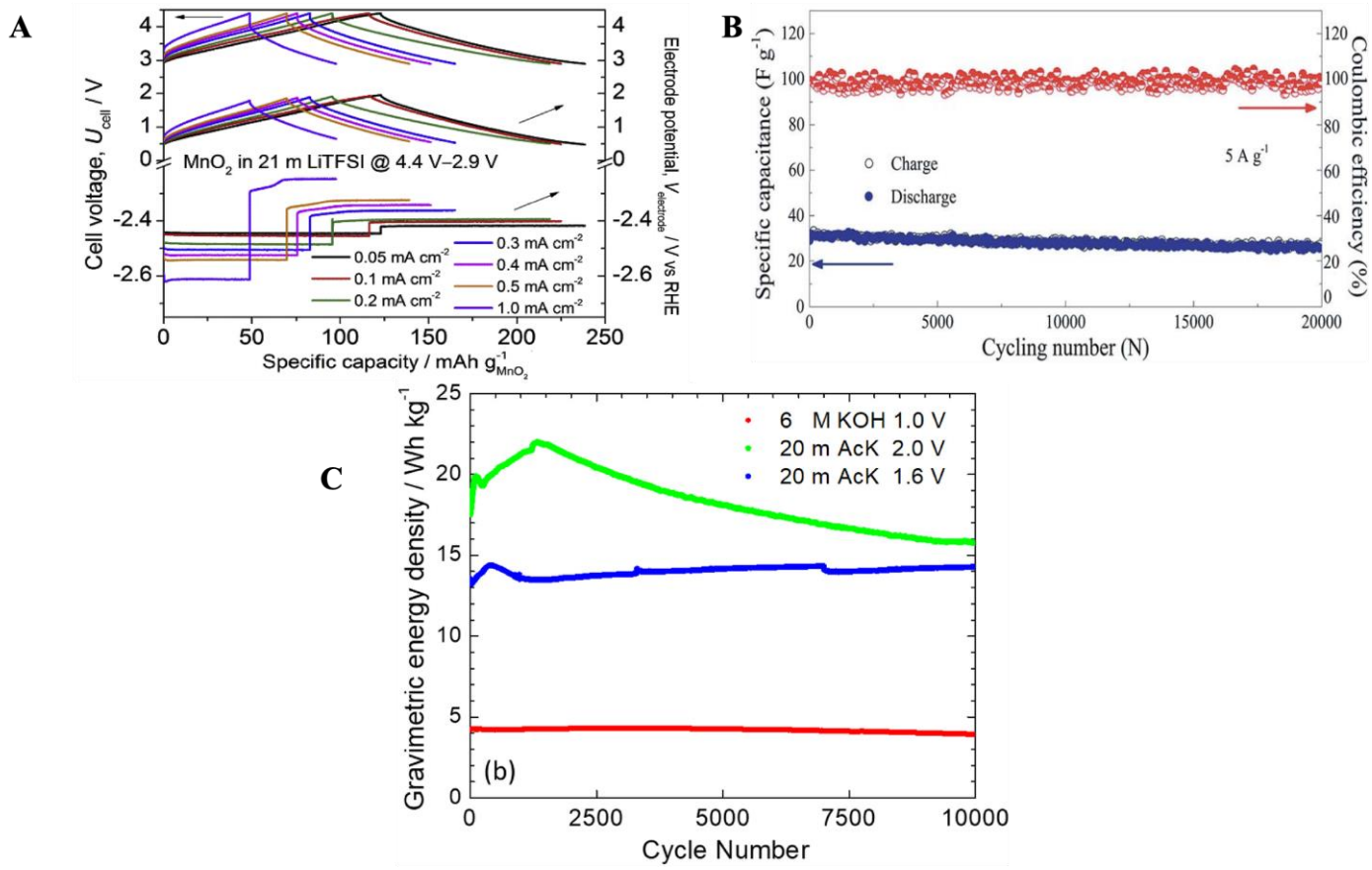

Figure 8. (**A**) GCD curve of a hybrid protected Li metal anode/MnO_2 cathode; Reprinted with permission from Ref. [73], Copyright 2018, Elsevier B.V. (**B**) long-term cycling performance of a 2.3 V YP-50F-based supercapacitor at a current density of 5 A g^{-1}; Reprinted with permission from Ref. [74], Copyright 2019, Royal Society of Chemistry (**C**) specific energy of symmetric F400 based supercapacitor in different electrolytes; Reprinted with permission from Ref. [75], Copyright 2020, Elsevier B.V.

The same group also developed a cost-effective Fe_3O_4/MnO_2-based aqueous device using 21 mol kg^{-1} LiTFSI as the electrolyte. This supercapacitor showed a cell voltage of 2.2 V, and a specific energy of 35.5 Wh kg^{-1} with a power density of 151.9 W kg^{-1}. The same group also developed a cost-effective Fe_3O_4/MnO_2-based aqueous device using 21 mol kg^{-1} LiTFSI as the electrolyte. This supercapacitor showed a cell voltage of 2.2 V, and a specific energy of 35.5 Wh kg^{-1} with a power density of 151.9 W kg^{-1} [76]. Other WIS electrolytes employed in supercapacitors included 17 mol kg^{-1} $NaClO_4$ and 12 mol kg^{-1} $NaNO_3$. The 17 mol kg^{-1} $NaClO_4$ WIS electrolyte was used in a symmetric supercapacitor based on YP-50F electrodes which showed a cell voltage of 2.3 V and capacitance of 33.0 F g^{-1} and 29.2 F g^{-1} at current density of 1 and 20 A g^{-1}, respectively. Figure 8B reports the long-term cycling performance of a 2.3 V YP-50F-based supercapacitor at a current density of 5 A g^{-1} [74]. Low-cost $NaNO_3$ 12 mol kg^{-1} WIS electrolyte was used in a symmetric capacitor based on YP-50F electrodes which showed a high cell voltage of 2.1 V with capacitance of 32.7 F g^{-1} and 25.2 F g^{-1} at current densities of 1 and 30 A g^{-1}, respectively [77]. Benefitting from the low cost and high solubility of KAc, our group recently investigated a symmetric supercapacitor based on free-standing activated carbon (F400) electrodes in a highly concentrated 20 mol kg^{-1} KAc aqueous electrolyte. This supercapacitor delivered a good specific energy of 26 Wh kg^{-1} (Figure 8C) and an average power of 1.4 kW kg^{-1} [75]. A list of various full cells enabled by WIS electrolytes together with their cell voltage, specific energy and performance is given in Table 2.

Table 2. Electrochemical performance of electrode couples used in different WIS electrolytes.

Electrode Couple	Electrolyte	ESW (V)	Collector Used	Cell Voltage (V)	Specific Energy (Wh kg^{-1})	Performance: Capacity Retention (CR) Capacity Decay (CD)	Ref.
$LiMn_2O_4/Mo_6S_8$	21 m LiTFSI	3	Stainless steel	2.3	100	68% CR at 4.5 C over 1000 cycles	[17]
$LiMn_2O_4/C–TiO_2$	21 m LiTFSI + 7 m LiOTF	3.07	Stainless steel	2.1	100	40 $mAhg^{-1}$ after 100 cycles	[23]
$LiMn_2O_4/C–TiO_2$	32 m KOAc + 8 m LiOAc	3	Ti	2.5	n.a.	90% CR after 100 cycles	[32]
$LiNi_{0.5}Mn_{1.5}O_4/Mo_6S_8$	21 m LiTFSI	4	3	2.9	126	n.a.	[47]
$LiNi_{0.5}Mn_{1.5}O_4/Li_4Ti_5O_{12}$	14 M LiTFSI + DMC	4.1	Al/Ti	3.2	165	0.024% CD for 1000 cycles (6 C)	[37]
$Li_4Ti_5O_{12}/LiMn_2O_4$	LiTFSI + 94%PEG + 6%H_2O	3.2	Coated Al	2.25	110	68% CR after 300 cycles.	[40]
$NaTi_2(PO_4)_3/Na_3(VOPO_4)_2F$	25 m NaFSI +10 m NaTFSI	2.7	n.a.	2	64	77% CR after 500 cycles at 1 C	[43]
$Na_{0.66}[Mn_{0.66}Ti_{0.34}]_{O2}/NaTi_2(PO_4)_3$	9.26 m $NaCF_3SO_3$	>2.5	Stainless steel	1	31	92.7% CR after 1200 cycles	[56]
$Na_3V_2(PO_4)_3/NaTi_2(PO_4)_3$	7 m NaOTF (H_2O) and 8 m NaOTF (propylene carbonate)	2.8	n.a.	1.2	45	20 mA h g^{-1} after 150 cycles (10 C)	[39]
$Na_4Fe_3(PO_4)_2(P_2O_7)/NaTi_2(PO_4)_3$	17 m $NaClO_4$	2.7	n.a.	2.0	36	65 mA h g^{-1} after 200 cycles (1 C)	[33]
$Zn/LiMn_2O_4$ hybrid battery	1 m Zn(TFSI)2 +20 m LiTFSI	n.a	n.a	1.4	70	85% CR after 4000 cycles	[65]
$Zn/LiMn_{0.8}Fe_{0.2}PO_4$	21 m of LiTFSI and 0.5 m of $ZnSO_4$	3.7	Stainless steel	1.8	183	110 mA h g^{-1} after 150 cycles (0.3 C)	[67]
$Zn/Ca_{0.2}0V_2O_5{\cdot}0.8H_2O$	30 m ZnCl2	1.8	n.a.	1.8	206	70% CR over 1000 cycles (1.6 A g^{-1})	[78]
Al/graphite	$AlCl_3{\cdot}6H_2O$	4	n..a	1.4	220	99% CR after 1000 cycles	[79]

The radar or spider chart is an easy and effective way of displaying multivariate data in a 2D chart of three or more variables. Radar charts based on important parameters such as cost, ionic conductivity, ESW, toxicity, and stability for various electrolytic systems are presented in Figure 9. Figure 9A summarizes some important alkaline ion-based electrolytes used for WIS-based lithium or sodium batteries. Two main classes of solutions can be found, based on the alkaline ion counter-anion: fluorinated electrolytes, which exploit the SEI formation, and cost-effective acetate-based electrolytes, which are less toxic, show similar performances, and are cost effective. In Figure 9B, different WIS electrolytes for sodium ion batteries are reported. Nitrates seem a good choice in terms of electrical properties and cost, but they suffer from chemical instability. Some important hybrid organic/inorganic electrolytes are summarized in Figure 9C which show good ESW at a lower cost. Although this approach seems very promising, a trade-off between electrical and electrochemical properties is present. Finally, some examples of electrolytes for other metal ion batteries cu Al, Zn, and Ca are presented in Figure 9D.

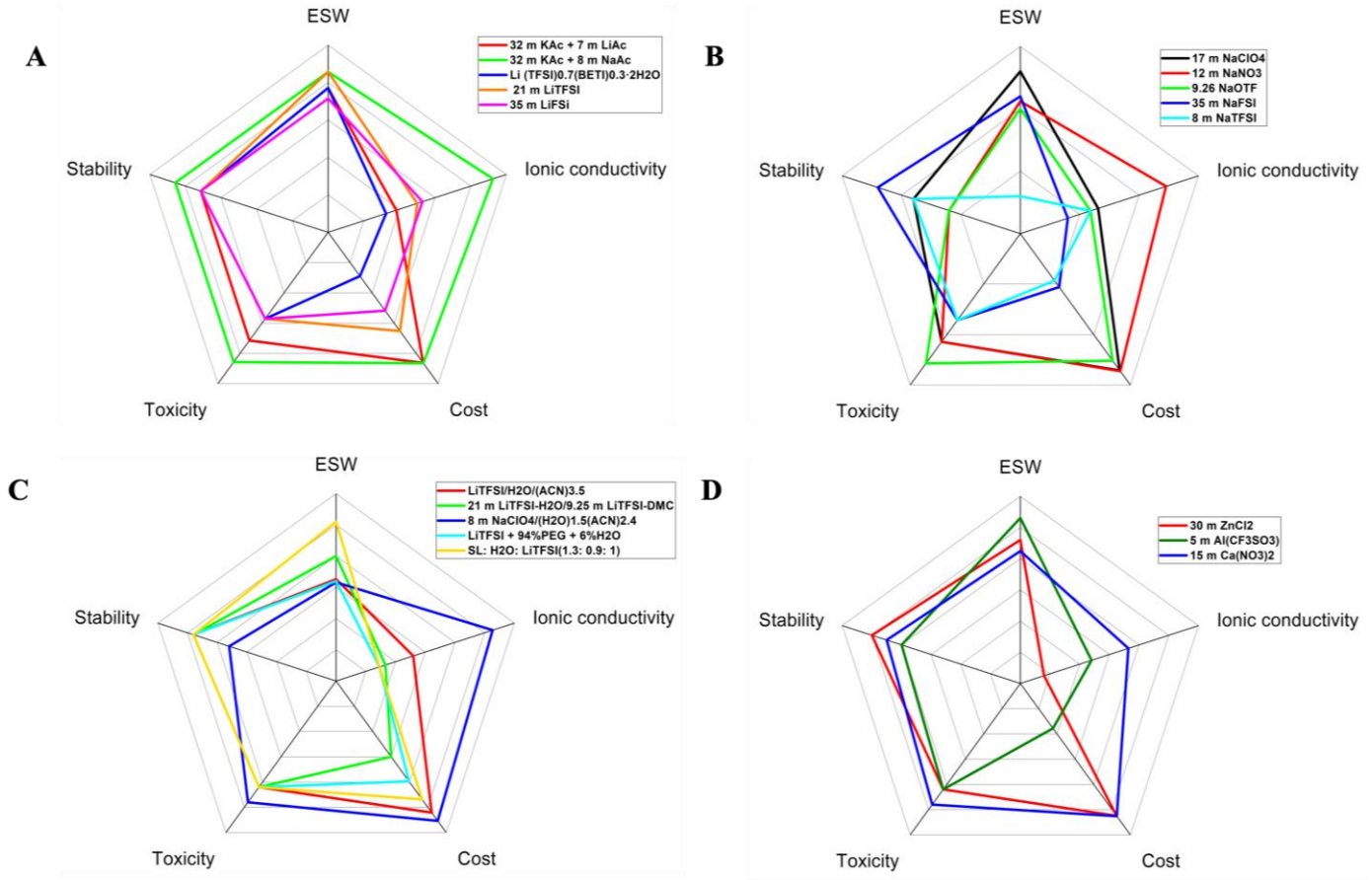

Figure 9. Radar charts of important parameters for various water in salt electrolytes. (**A**) WIS electrolytes for lithium/sodium chemistries based on binary salts; (**B**) WIS electrolytes for sodium-based chemistries; (**C**) Hybrid organic/aqueous electrolytes for lithium/sodium chemistries; (**D**) other metal ion chemistries such as aluminum, zinc, calcium.

4. Technological Perspectives

Batteries are a fundamental part of today's society powering essential aspects of daily life such as communication, transportation, and energy storage. LIB technology dominates today's market, but it still suffers from some issues which indeed need improvement. One direction in this effort is research in rechargeable aqueous batteries. Water is not only nonflammable, but also has good dielectric constant and can dissolve many cost-effective salts at a high concentration which enhances the conductivity and allows high-rate operation. Moreover, water is readily accessible and easy to handle, thus, we can expect a lower initial fixed cost for a dry room installation/maintenance from an industrial viewpoint. As shown in the previous sections, a range of cost-effective solutions can be created for different applications using water as a versatile platform. In this section, we will focus on the technological perspectives of aqueous batteries in different application areas, such as the grid, automotive industry, low-cost electronics, and backup applications [80]. We will focus our attention on the crucial requirements in various application areas, which are listed in order of relevance into parentheses in the paragraphs' titles.

4.1. Portable Electronics (Energy, Safety, Cycles)

The world is becoming more portable due to the high demand for the efficient collection and transfer of global information, which requires an advanced portable information exchange platform to allow immediate responses. Portable Electronic Devices (PEDs) such as mobile phones, laptops/tablets, digital cameras, consumer drones and wearable electronics (smart watches, smart glasses, smart clothing, etc.) revolutionized the progress in

information and data sharing. Modern multifunctional PEDs have high energy consumption, therefore the battery requirements include high energy, longer operational time, lighter weight, and smaller volume, whereas power density is not a crucial constraint [81,82]. Since 1991 [83], the Li-ion battery remains the choice for modern-day PEDs due to its high specific energy, low discharge rates, good life span, no maintenance, and high voltage. However, the safety of LIBs is posing concerns due to the flammable nature of liquid electrolytes. Moreover, the manufacturing cost of LIBs is still high compared to other rechargeable batteries although it is decreasing year by year. A solution to the safety problem is to use solid electrolytes, or to move towards aqueous-based batteries. The scientific community has greatly worked on aqueous electrolytes for highly safe and fast Li-ion batteries, but the specific energy of the investigated examples is still low to replace the benchmark LIBs based on organic electrolytes. Together with aqueous LIBs, other battery chemistries such as aqueous Na-ion, K-ion, and zinc metal batteries are in their initial phases of development which may replace the current choice of battery technology for PEDs.

4.2. Grid Applications (Quickness, Safety, Cost)

Energy from renewable sources such as solar and wind is significant, but greatly dependent on time and place. The intermittent nature of these energy sources makes it very difficult to integrate them directly into the power grid. Alternatively, the energy produced from these sources can be stored in large grid-scale energy storage systems which act as a buffer to keep a balance between demand and power supply. There are two important requirements for grid-scale energy storage systems: (i) high-rate performance, and (ii) safety. As a grid power stabilizer, the energy storage system should be able to respond quickly (<20 ms) to the fluctuations in a grid which means high-rate capability is needed on the battery part. Moreover, a grid-scale energy storage system will be made of many battery modules. Therefore, even a small accident in the energy storage system can have catastrophic consequences in its surroundings. Luckily, grid-scale applications of energy storage systems are not sensitive to specific energy because of their big scale and stationary nature. This low sensitivity to specific energy is a huge relief for the present aqueous battery systems owing to their lower energy densities compared to Li-ion batteries. Moreover, the recent fire accidents related to Li-ion batteries made safety a primary concern. In addition, from an economic point of view, Li-ion batteries for stationary applications are still too expensive. Therefore, novel energy storage systems are urgently needed to fulfill the requirements for grid application. The lead acid battery is the cheapest option, but it suffers from the issues of efficiency, life span, etc. Flow batteries and Na-S batteries are hampered by low-rate capability and poor efficiency. Carnegie Mellon University and Aquion Energy (https://www.aquionenergy.com/company/accessed on 15 November 2022) are investigating an aqueous sodium-ion battery for power grid application. The Massachusetts Institute of Technology is investigating a cost-effective all-liquid metal battery for grid application [84]. The Fluidic energy corporation in Arizona supported by the US energy department is working on a Zn-air battery based on ionic liquid electrolytes [84]. Aqueous Zn-ion batteries are believed to fit the needs of the grid application due to their low cost, high-rate performance, and safety. Gas evolution due to electrolyte depletion could limit the cyclic performance of aqueous Zn-ion batteries due to a continuous gas pressure build-up. This problem can be negligible at the laboratory scale, but it will be a problem for extended grid applications. Therefore, suppression of gas evolution and degassing strategies are required to ensure the practical use of these energy systems. It is evident that in grid applications the use of batteries based on ESW-extended WIS electrolytes is very promising. Devices based on WIS electrolytes, indeed, can offer advantages in terms of specific energy and safety, but the high cost of the electrolyte is the main bottleneck in using them for a practical application on a big scale such as a power grid [85,86].

4.3. Power Back-Up (Energy, Quickness, Cost)

The uninterruptable power source (UPS) is an electrical device that provides emergency power to electronic devices when the main power supply is interrupted. UPSs find applications in computer systems, telecommunication, data storage, medical facilities, industrial processing, etc. Batteries were used in UPS systems for a long time, guaranteeing a stable power supply during power outages. The energy storage capacity of these electrochemical batteries mostly governs the performance of UPS systems. Historically, lead acid batteries, particularly the valve-regulated lead acid battery (VRLAB), has been widely adopted in UPS applications because of low cost, and low internal impedance. However, lead acid batteries have a life span of fewer than 1000 cycles and require extensive maintenance and replacement which may increase the cost of a UPS. The Ni-Cd technology remained a popular choice for the telecom sector, and it is used in UPS applications in areas with high ambient temperatures. The Ni-Cd battery offers an extended cycle life and wide temperature operation but is very expensive compared to common VRLABs used for the same application. In addition, the presence of elements such as nickel and cadmium make their recycling very expensive.

LIB technology is increasingly becoming a viable option for UPS and other small energy storage systems as it offers remarkably higher energy density compared to the traditional batteries. Moreover, LIBs also have better cycle life, faster charging time, and double service life compared to lead acid or Ni-Cd batteries. Despite the decrease in the cost of Li-ion cells, their use in UPS is still an expensive choice compared to the other technologies, and lead acid battery is expected to remain cheaper for the next two decades than its alternatives [87].

Because of the balance between performance and safety, WIS electrolyte batteries could be commonly applied in this area. In fact, they already have higher performance than common lead-acid batteries and fewer problems than LIBs. The bottleneck to overcome here is indeed cost, especially regarding fluorinated systems. However, we have shown how WIS batteries based on acetates can be viable alternatives, not to mention that the costs of fluorinated salts could be significantly lower due to economy of scale and the fact that they do not need to be used anhydrous.

4.4. Automotive (Energy/Power Density, Safety, Life Cycle, Cost)

Indeed, the automotive sector is the most demanding for the next generation EESSs and will revolutionize modern day transportation in terms safety, ease, cost, and environment. Global demand for electric vehicles (EVs) has rapidly increased during the past five years and is expected to rise exponentially in the next decades. An analysis done by Fitch [88] in 2021 forecasted that the global sale of electric vehicles will increase to 26.7 million in 2030 with a yearly increase of 379% from the year 2021. In this context, the analysis also forecasted that the global annual demand for batteries in the EV industry in terms of capacity will increase to an astonishing 1925 GWh in 2030 which will be a 688% increase from a of value 244 GWh for the year 2021. According to the Bloomberg NEF (BNEF) report [89], the cost of a Li-ion battery pack has decreased by 89% from 1200 \$ kWh^{-1} to 132 \$ kWh^{-1} in 2021. The BNEF survey for the year 2021 has predicted that the overall cost of a battery pack would fall below the value of 100 \$ kWh^{-1} [90].

The current generation (Gen 2) commercial Li-ion battery technology has a specific energy ranging 90–235 Wh kg^{-1}. The advanced batteries (Gen 3) are expected to reach the target specific energy of 350 Wh kg^{-1} in the year 2025 while the goal for the 4th generation is 500 Wh kg^{-1} or 1000 Wh L^{-1}. Considering the specific energy and energy density requirements (90–235 Wh kg^{-1} and 200–600 Wh L^{-1}) for EVs even for the current Gen 2 LIBs, the aqueous battery chemistries are yet out of the race [88].

However, although the use of organic electrolytes ensures the high energy density of the batteries in EV applications, the highly flammable nature of nonaqueous electrolytes is a serious safety concern. The presence of high-energy electrodes and highly flammable electrolytes in the battery pack of EVs can result in a catastrophic fire in case of an accident. A so-

lution to this safety hazard in the current commercial LIB technology is to replace flammable electrolytes with nonflammable ones. In this sense, water or hybrid organic/water solvent mixtures are the best alternative. Established aqueous battery chemistries such as lead acid, Ni-Cd, and Ni-metal hydride are limited primarily by their low energy density compared to the current LIBs. The first Li-ion aqueous battery demonstrated by Dahn et al. [26] employed V_2O_5 and $LiMn_2O_4$ in a 5 m $LiNO_3$ aqueous electrolyte, and had an specific energy of 55 Wh kg^{-1} comparable to that of a VRLAB. This specific energy is very low compared to the target energy densities for next-generation long-range EVs.

Highly concentrated hybrid/aqueous electrolytes working beyond the water thermodynamic stability limit achieved handsome energy density with good rate performance due to the high conductivity and the possibility to use LIB electrodes. Important examples include various electrode couples mentioned in Table 2. Energy densities of more than 100 Wh kg^{-1} for many of the hybrid WIS-based cells were recorded. To date, the highest specific energy values recorded for aqueous electrolytes is 165 Wh kg^{-1} and 173 Wh kg^{-1} for the DMC/H_2O/LiTFSI and LiTFSI/H_2O/acetonitrile-based electrolytes, respectively [38,39]. Even if these specific energy values are good for an aqueous electrolyte-based device, they are still far below the goal required for automotive applications. Other battery chemistries that could be promising in the application of EVs could be aqueous Zn- and Al-based systems. However, at present, the research on these chemistries is still in its infancy. Conclusively, the pace of progress toward more energy-dense batteries seems to proceed with the current organic-based Li-ion chemistries for the EVs application in the near future [63].

5. Conclusions

Aqueous secondary ion batteries are emerging as promising energy storage systems, especially for intermittent energy usage and stationary large-scale applications. The affordable cost, easy processing, abundant resources, eco-friendliness, and most importantly, the safety of these advanced aqueous batteries make them a viable option to replace the conventional lead-acid, nickel metal hydride, and Li-ion batteries. There has been a rapid increase in research regarding aqueous systems in the past decade. Several strategies have been developed to expand the ESW of aqueous electrolytes such as: (i) using SEI promoters like TFSI, FSI, and other fluorinated anions; (ii) by reducing water activity, and (iii) using aqueous/nonaqueous hybrid approaches. Each of these approaches comes with its own pros and cons. For instance, the SEI promoters i.e., the fluorinated systems, have the best stability due to the SEI formation as a result of the reductive decomposition of fluorinated species, but this approach suffers from the issues of high cost and environmental concerns. Much progress was made with the cost-effective acetates salts to reduce the activity of water molecules by super-concentration. The performance of aqueous batteries reached a new pinnacle with the use of a hybrid approach i.e., by combining aqueous and organic components inheriting the properties of safety from the aqueous part and stability from the organic part.

However, these approaches are still at the prototype level, and although there are a lot of examples of full cells, these are at TRL < 6, being only validated in the technologically relevant environments. A direct comparison of WIS performance with commercial technologies should therefore be made at the materials level instead then at the cell level. For this reason, and to better envisage the state-of-the-art, we constructed the Ragone plot in Figure 10 using data from some of the works considered in this paper and using state-of-the-art LIBs and supercaps as a comparison. The Ragone plot shows that WIS batteries still suffer of a performance gap compared to LIBs, therefore their development should be directed toward applications where performance is not prioritized over safety and cost, such as grid energy storage (for high-power systems). Instead, an interesting role could be played in specific supercapacitors applications, where WIS devices perform similarly to traditional devices.

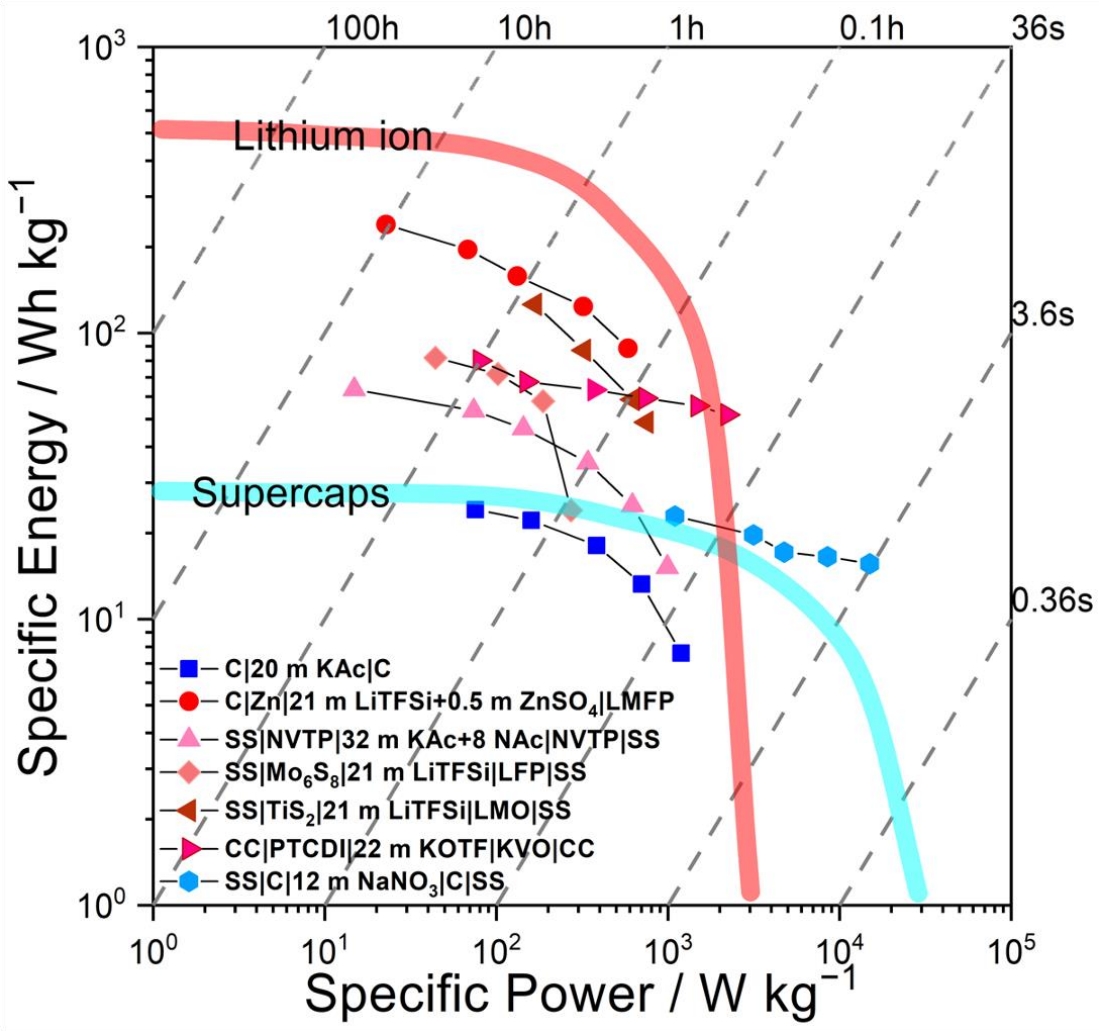

Figure 10. Ragone plot of several WIS full cells cited in this work. Specific energy and specific power have been calculated at the materials level, using the total amount of active material. Battery-like cells are in different shades of red, supercaps in blue. For the sake of comparison, traditional LIBs and supercaps are also shown calculated at the materials level. [75], [67], [17], [46], [49], , [77].

Author Contributions: Conceptualization, S.K. and R.R.; methodology, S.K. and N.P.; data curation, N.P.; writing—original draft preparation, S.K.; writing—review and editing, S.K. and P.M.; visualization, all authors; supervision, R.R.; project administration, P.M.; funding acquisition, R.R. All authors have read and agreed to the published version of the manuscript.

Funding: This research was funded by ENI Spa, under the Joint Research Agreement ENI-Università di Milano Bicocca grant number Nr. 5210001818.

Data Availability Statement: No new research data were created for this article. All shown data were collected from literature and their availability depends on the restrictions applied to the original works.

Conflicts of Interest: The authors declare no conflict of interest.

References

1. Kamat, P.V. Lithium-Ion Batteries and Beyond: Celebrating the 2019 Nobel Prize in Chemistry—A Virtual Issue. *ACS Energy Lett.* **2019**, *4*, 2757–2759. [CrossRef]
2. Xie, J.; Lu, Y.-C. A retrospective on lithium-ion batteries. *Nat. Commun.* **2020**, *11*, 2499. [CrossRef]
3. Vincent, C.A. Lithium batteries: A 50-year perspective, 1959–2009. *Solid State Ion.* **2000**, *134*, 159–167. [CrossRef]
4. Wang, Q.; Jiang, L.; Yu, Y.; Sun, J. Progress of enhancing the safety of lithium ion battery from the electrolyte aspect. *Nano Energy* **2018**, *55*, 93–114. [CrossRef]
5. Hou, J.; Yang, M.; Wang, D.; Zhang, J. Fundamentals and Challenges of Lithium Ion Batteries at Temperatures between −40 and 60 °C. *Adv. Energy Mater.* **2020**, *10*, 1904152. [CrossRef]
6. Dey, A.N.; Sullivan, B.P. The Electrochemical Decomposition of Propylene Carbonate on Graphite. *J. Electrochem. Soc.* **1970**, *117*, 222–224. [CrossRef]
7. Peled, E. The Electrochemical Behavior of Alkali and Alkaline Earth Metals in Nonaqueous Battery Systems—The Solid Electrolyte Interphase Model. *J. Electrochem. Soc.* **1979**, *126*, 2047–2051. [CrossRef]
8. Xu, K. Nonaqueous Liquid Electrolytes for Lithium-Based Rechargeable Batteries. *Chem. Rev.* **2004**, *104*, 4303–4418. [CrossRef]
9. Kim, H.; Hong, J.; Park, K.-Y.; Kim, H.; Kim, S.-W.; Kang, K. Aqueous Rechargeable Li and Na Ion Batteries. *Chem. Rev.* **2014**, *114*, 11788–11827. [CrossRef]
10. Hu, L.; Xu, K. Nonflammable electrolyte enhances battery safety. *Proc. Natl. Acad. Sci. USA* **2014**, *111*, 3205–3206. [CrossRef]
11. Liang, T.; Hou, R.; Dou, Q.; Zhang, H.; Yan, X. The Applications of Water-in-Salt Electrolytes in Electrochemical Energy Storage Devices. *Adv. Funct. Mater.* **2021**, *31*, 2006749. [CrossRef]
12. Droguet, L.; Grimaud, A.; Fontaine, O.; Tarascon, J. Water-in-Salt Electrolyte (WiSE) for Aqueous Batteries: A Long Way to Practicality. *Adv. Energy Mater.* **2020**, *10*, 2002440. [CrossRef]
13. Mankowski, P.J.; Kanevsky, J.; Bakirtzian, P.; Cugno, S. Cellular phone collateral damage: A review of burns associated with lithium battery powered mobile devices. *Burns* **2016**, *42*, e61–e64. [CrossRef] [PubMed]
14. Ratner, M.A.; Shriver, D.F. Ion transport in solvent-free polymers. *Chem. Rev.* **1988**, *88*, 109–124. [CrossRef]
15. Angell, C.A.; Liu, C.; Sanchez, E. Rubbery solid electrolytes with dominant cationic transport and high ambient conductivity. *Nature* **1993**, *362*, 137–139. [CrossRef]
16. McKinnon, W.R.; Dahn, J.R. How to Reduce the Cointercalation of Propylene Carbonate in Li x ZrS2 and Other Layered Compounds. *J. Electrochem. Soc.* **1985**, *132*, 364–366. [CrossRef]
17. Suo, L.; Borodin, O.; Gao, T.; Olguin, M.; Ho, J.; Fan, X.; Luo, C.; Wang, C.; Xu, K. "Water-in-salt" electrolyte enables high-voltage aqueous lithium-ion chemistries. *Science* **2015**, *350*, 938–943. [CrossRef]
18. Dubouis, N.; Lemaire, P.; Mirvaux, B.; Salager, E.; Deschamps, M.; Grimaud, A. The role of the hydrogen evolution reaction in the solid–electrolyte interphase formation mechanism for "*Water-in-Salt*" electrolytes. *Energy Environ. Sci.* **2018**, *11*, 3491–3499. [CrossRef]
19. Li, M.; Wang, C.; Chen, Z.; Xu, K.; Lu, J. New Concepts in Electrolytes. *Chem. Rev.* **2020**, *120*, 6783–6819. [CrossRef]
20. Yang, C.; Chen, J.; Qing, T.; Fan, X.; Sun, W.; von Cresce, A.; Ding, M.S.; Borodin, O.; Vatamanu, J.; Schroeder, M.; et al. 4.0 V Aqueous Li-Ion Batteries. *Joule* **2017**, *1*, 122–132. [CrossRef]
21. Suo, L.; Oh, D.; Lin, Y.; Zhuo, Z.; Borodin, O.; Gao, T.; Wang, F.; Kushima, A.; Wang, Z.; Kim, H.-C.; et al. How Solid-Electrolyte Interphase Forms in Aqueous Electrolytes. *J. Am. Chem. Soc.* **2017**, *139*, 18670–18680. [CrossRef] [PubMed]
22. Chao, D.; Zhou, W.; Xie, F.; Ye, C.; Li, H.; Jaroniec, M.; Qiao, S.-Z. Roadmap for advanced aqueous batteries: From design of materials to applications. *Sci. Adv.* **2020**, *6*, eaba4098. [CrossRef] [PubMed]
23. Suo, L.; Borodin, O.; Sun, W.; Fan, X.; Yang, C.; Wang, F.; Gao, T.; Ma, Z.; Schroeder, M.; von Cresce, A.; et al. Advanced High-Voltage Aqueous Lithium-Ion Battery Enabled by "Water-in-Bisalt" Electrolyte. *Angew. Chem. Int. Ed.* **2016**, *55*, 7136–7141. [CrossRef] [PubMed]
24. Hosaka, T.; Kubota, K.; Kojima, H.; Komaba, S. Highly concentrated electrolyte solutions for 4 V class potassium-ion batteries. *Chem. Commun.* **2018**, *54*, 8387–8390. [CrossRef]
25. Li, W.; McKinnon, W.R.; Dahn, J.R. Lithium Intercalation from Aqueous Solutions. *J. Electrochem. Soc.* **1994**, *141*, 2310–2316. [CrossRef]
26. Li, W.; Dahn, J.R.; Wainwright, D.S. Rechargeable Lithium Batteries with Aqueous Electrolytes. *Science* **1994**, *264*, 1115–1118. [CrossRef]
27. Li, W.; Dahn, J.R. Lithium-Ion Cells with Aqueous Electrolytes. *J. Electrochem. Soc.* **1995**, *142*, 1742–1746. [CrossRef]
28. Lux, S.F.; Terborg, L.; Hachmöller, O.; Placke, T.; Meyer, H.-W.; Passerini, S.; Winter, M.; Nowak, S. LiTFSI Stability in Water and Its Possible Use in Aqueous Lithium-Ion Batteries: pH Dependency, Electrochemical Window and Temperature Stability. *J. Electrochem. Soc.* **2013**, *160*, A1694–A1700. [CrossRef]
29. Kulkarni, P.; Ghosh, D.; Balakrishna, R.G. Recent progress in 'water-in-salt' and 'water-in-salt'-hybrid-electrolyte-based high voltage rechargeable batteries. *Sustain. Energy Fuels* **2021**, *5*, 1619–1654. [CrossRef]
30. Becker, M.; Kühnel, R.-S.; Battaglia, C. Water-in-salt electrolytes for aqueous lithium-ion batteries with liquidus temperatures below −10 °C. *Chem. Commun.* **2019**, *55*, 12032–12035. [CrossRef]
31. Reber, D.; Figi, R.; Kühnel, R.-S.; Battaglia, C. Stability of aqueous electrolytes based on LiFSI and NaFSI. *Electrochim. Acta* **2019**, *321*, 134644. [CrossRef]

32. Lukatskaya, M.R.; Feldblyum, J.I.; Mackanic, D.G.; Lissel, F.; Michels, D.L.; Cui, Y.; Bao, Z. Concentrated mixed cation acetate "water-in-salt" solutions as green and low-cost high voltage electrolytes for aqueous batteries. *Energy Environ. Sci.* **2018**, *11*, 2876–2883. [CrossRef]
33. Lee, M.H.; Kim, S.J.; Chang, D.; Kim, J.; Moon, S.; Oh, K.; Park, K.-Y.; Seong, W.M.; Park, H.; Kwon, G.; et al. Toward a low-cost high-voltage sodium aqueous rechargeable battery. *Mater. Today* **2019**, *29*, 26–36. [CrossRef]
34. Han, J.; Zhang, H.; Varzi, A.; Passerini, S. Fluorine-Free Water-in-Salt Electrolyte for Green and Low-Cost Aqueous Sodium-Ion Batteries. *Chemsuschem* **2018**, *11*, 3704–3707. [CrossRef]
35. Stigliano, P.L.; Pianta, N.; Bonizzoni, S.; Mauri, M.; Simonutti, R.; Lorenzi, R.; Vigani, B.; Berbenni, V.; Rossi, S.; Mustarelli, P.; et al. A physico-chemical investigation of highly concentrated potassium acetate solutions towards applications in electrochemistry. *Phys. Chem. Chem. Phys.* **2021**, *23*, 1139–1145. [CrossRef]
36. Khalid, S.; Pianta, N.; Bonizzoni, S.; Mustarelli, P.; Ruffo, R. The properties of highly concentrated aqueous CH3COOK/Na binary electrolyte and its use in sodium-ion batteries. *ChemRxiv* **2021**. [CrossRef]
37. Wang, F.; Borodin, O.; Ding, M.S.; Gobet, M.; Vatamanu, J.; Fan, X.; Gao, T.; Eidson, N.; Liang, Y.; Sun, W.; et al. Hybrid Aqueous/Non-aqueous Electrolyte for Safe and High-Energy Li-Ion Batteries. *Joule* **2018**, *2*, 927–937. [CrossRef]
38. Chen, J.; Vatamanu, J.; Xing, L.; Borodin, O.; Chen, H.; Guan, X.; Liu, X.; Xu, K.; Li, W. Improving Electrochemical Stability and Low-Temperature Performance with Water/Acetonitrile Hybrid Electrolytes. *Adv. Energy Mater.* **2020**, *10*, 1902654. [CrossRef]
39. Zhang, H.; Qin, B.; Han, J.; Passerini, S. Aqueous/Nonaqueous Hybrid Electrolyte for Sodium-Ion Batteries. *ACS Energy Lett.* **2018**, *3*, 1769–1770. [CrossRef]
40. Xie, J.; Liang, Z.; Lu, Y.-C. Molecular crowding electrolytes for high-voltage aqueous batteries. *Nat. Mater.* **2020**, *19*, 1006–1011. [CrossRef]
41. Liu, J.; Yang, C.; Chi, X.; Wen, B.; Wang, W.; Liu, Y. Water/Sulfolane Hybrid Electrolyte Achieves Ultralow-Temperature Operation for High-Voltage Aqueous Lithium-Ion Batteries. *Adv. Funct. Mater.* **2022**, *32*, 2106811. [CrossRef]
42. Liu, D.; Yuan, L.; Li, X.; Chen, J.; Xiong, R.; Meng, J.; Zhu, S.; Huang, Y. Tuning the Electrolyte Solvation Structure via a Nonaqueous Co-Solvent to Enable High-Voltage Aqueous Lithium-Ion Batteries. *ACS Appl. Mater. Interfaces* **2022**, *14*, 17585–17593. [CrossRef] [PubMed]
43. Reber, D.; Kühnel, R.-S.; Battaglia, C. Suppressing Crystallization of Water-in-Salt Electrolytes by Asymmetric Anions Enables Low-Temperature Operation of High-Voltage Aqueous Batteries. *ACS Mater. Lett.* **2019**, *1*, 44–51. [CrossRef]
44. Xiao, D.; Dou, Q.; Zhang, L.; Ma, Y.; Shi, S.; Lei, S.; Yu, H.; Yan, X. Optimization of Organic/Water Hybrid Electrolytes for High-Rate Carbon-Based Supercapacitor. *Adv. Funct. Mater.* **2019**, *29*, 1904136. [CrossRef]
45. Dou, Q.; Lu, Y.; Su, L.; Zhang, X.; Lei, S.; Bu, X.; Liu, L.; Xiao, D.; Chen, J.; Shi, S.; et al. A sodium perchlorate-based hybrid electrolyte with high salt-to-water molar ratio for safe 2.5 V carbon-based supercapacitor. *Energy Storage Mater.* **2019**, *23*, 603–609. [CrossRef]
46. Suo, L.; Han, F.; Fan, X.; Liu, H.; Xu, K.; Wang, C. "Water-in-Salt" electrolytes enable green and safe Li-ion batteries for large scale electric energy storage applications. *J. Mater. Chem. A* **2016**, *4*, 6639–6644. [CrossRef]
47. Wang, F.; Suo, L.; Liang, Y.; Yang, C.; Han, F.; Gao, T.; Sun, W.; Wang, C. Spinel LiNi0.5Mn1.5O4 Cathode for High-Energy Aqueous Lithium-Ion Batteries. *Adv. Energy Mater.* **2017**, *7*, 1600922. [CrossRef]
48. Luo, J.-Y.; Xia, Y.-Y. Aqueous Lithium-ion Battery LiTi2(PO4)3/LiMn2O4 with High Power and Energy Densities as well as Superior Cycling Stability**. *Adv. Funct. Mater.* **2007**, *17*, 3877–3884. [CrossRef]
49. Sun, W.; Suo, L.; Wang, F.; Eidson, N.; Yang, C.; Han, F.; Ma, Z.; Gao, T.; Zhu, M.; Wang, C. "Water-in-Salt" electrolyte enabled LiMn2O4/TiS2 Lithium-ion batteries. *Electrochem. Commun.* **2017**, *82*, 71–74. [CrossRef]
50. Ramanujapuram, A.; Gordon, D.; Magasinski, A.; Ward, B.; Nitta, N.; Huang, C.; Yushin, G. Degradation and stabilization of lithium cobalt oxide in aqueous electrolytes. *Energy Environ. Sci.* **2016**, *9*, 1841–1848. [CrossRef]
51. Wang, L.; Chen, B.; Ma, J.; Cui, G.; Chen, L. Reviving lithium cobalt oxide-based lithium secondary batteries-toward a higher energy density. *Chem. Soc. Rev.* **2018**, *47*, 6505–6602. [CrossRef] [PubMed]
52. Lyu, Y.; Wu, X.; Wang, K.; Feng, Z.; Cheng, T.; Liu, Y.; Wang, M.; Chen, R.; Xu, L.; Zhou, J.; et al. An Overview on the Advances of $LiCoO_2$ Cathodes for Lithium-Ion Batteries. *Adv. Energy Mater.* **2021**, *11*, 2000982. [CrossRef]
53. Chen, Z.; Dahn, J. Methods to obtain excellent capacity retention in LiCoO2 cycled to 4.5 V. *Electrochim. Acta* **2004**, *49*, 1079–1090. [CrossRef]
54. Wang, F.; Lin, Y.; Suo, L.; Fan, X.; Gao, T.; Yang, C.; Han, F.; Qi, Y.; Xu, K.; Wang, C. Stabilizing high voltage $LiCoO_2$ cathode in aqueous electrolyte with interphase-forming additive. *Energy Environ. Sci.* **2016**, *9*, 3666–3673. [CrossRef]
55. Yamada, Y.; Usui, K.; Sodeyama, K.; Ko, S.; Tateyama, Y.; Yamada, A. Hydrate-melt electrolytes for high-energy-density aqueous batteries. *Nat. Energy* **2016**, *1*, 16129. [CrossRef]
56. Suo, L.; Borodin, O.; Wang, Y.; Rong, X.; Sun, W.; Fan, X.; Xu, S.; Schroeder, M.A.; Cresce, A.V.; Wang, F.; et al. "Water-in-Salt" Electrolyte Makes Aqueous Sodium-Ion Battery Safe, Green, and Long-Lasting. *Adv. Energy Mater.* **2017**, *7*, 1701189. [CrossRef]
57. Han, J.; Zarrabeitia, M.; Mariani, A.; Jusys, Z.; Hekmatfar, M.; Zhang, H.; Geiger, D.; Kaiser, U.; Behm, R.; Varzi, A.; et al. Halide-free water-in-salt electrolytes for stable aqueous sodium-ion batteries. *Nano Energy* **2020**, *77*, 105176. [CrossRef]
58. Leonard, D.P.; Wei, Z.; Chen, G.; Du, F.; Ji, X. Water-in-Salt Electrolyte for Potassium-Ion Batteries. *ACS Energy Lett.* **2018**, *3*, 373–374. [CrossRef]

59. Jiang, L.; Lu, Y.; Zhao, C.; Liu, L.; Zhang, J.; Zhang, Q.; Shen, X.; Zhao, J.; Yu, X.; Li, H.; et al. Building aqueous K-ion batteries for energy storage. *Nat. Energy* **2019**, *4*, 495–503. [CrossRef]
60. Liu, T.; Tang, L.; Luo, H.; Cheng, S.; Liu, M. A promising water-in-salt electrolyte for aqueous based electrochemical energy storage cells with a wide potential window: Highly concentrated HCOOK. *Chem. Commun.* **2019**, *55*, 12817–12820. [CrossRef]
61. Chen, H.; Zhang, Z.; Wei, Z.; Chen, G.; Yang, X.; Wang, C.; Du, F. Use of a water-in-salt electrolyte to avoid organic material dissolution and enhance the kinetics of aqueous potassium ion batteries. *Sustain. Energy Fuels* **2019**, *4*, 128–131. [CrossRef]
62. Liang, G.; Gan, Z.; Wang, X.; Jin, X.; Xiong, B.; Zhang, X.; Chen, S.; Wang, Y.; He, H.; Zhi, C. Reconstructing Vanadium Oxide with Anisotropic Pathways for a Durable and Fast Aqueous K-Ion Battery. *ACS Nano* **2021**, *15*, 17717–17728. [CrossRef] [PubMed]
63. Ponrouch, A.; Bitenc, J.; Dominko, R.; Lindahl, N.; Johansson, P.; Palacin, M. Multivalent rechargeable batteries. *Energy Storage Mater.* **2019**, *20*, 253–262. [CrossRef]
64. Fang, G.; Zhou, J.; Pan, A.; Liang, S. Recent Advances in Aqueous Zinc-Ion Batteries. *ACS Energy Lett.* **2018**, *3*, 2480–2501. [CrossRef]
65. Wang, F.; Borodin, O.; Gao, T.; Fan, X.; Sun, W.; Han, F.; Faraone, A.; Dura, J.A.; Xu, K.; Wang, C. Highly reversible zinc metal anode for aqueous batteries. *Nat. Mater.* **2018**, *17*, 543–549. [CrossRef] [PubMed]
66. Hu, P.; Yan, M.; Zhu, T.; Wang, X.; Wei, X.; Li, J.; Zhou, L.; Li, Z.; Chen, L.; Mai, L. Zn/V_2O_5 Aqueous Hybrid-Ion Battery with High Voltage Platform and Long Cycle Life. *ACS Appl. Mater. Interfaces* **2017**, *9*, 42717–42722. [CrossRef] [PubMed]
67. Zhao, J.; Li, Y.; Peng, X.; Dong, S.; Ma, J.; Cui, G.; Chen, L. High-voltage Zn/LiMn0.8Fe0.2PO4 aqueous rechargeable battery by virtue of "water-in-salt" electrolyte. *Electrochem. Commun.* **2016**, *69*, 6–10. [CrossRef]
68. Zhang, C.; Holoubek, J.; Wu, X.; Daniyar, A.; Zhu, L.; Chen, C.; Leonard, D.P.; Rodríguez-Pérez, I.A.; Jiang, J.-X.; Fang, C.; et al. A $ZnCl_2$ water-in-salt electrolyte for a reversible Zn metal anode. *Chem. Commun.* **2018**, *54*, 14097–14099. [CrossRef]
69. Lee, C.; Jeong, S.-K. A Novel Superconcentrated Aqueous Electrolyte to Improve the Electrochemical Performance of Calcium-ion Batteries. *Chem. Lett.* **2016**, *45*, 1447–1449. [CrossRef]
70. Adil; Ghosh, A.; Mitra, S. Water-in-Salt Electrolyte-Based Extended Voltage Range, Safe, and Long-Cycle-Life Aqueous Calcium-Ion Cells. *ACS Appl. Mater. Interfaces* **2022**, *14*, 25501–25515. [CrossRef]
71. Leong, K.W.; Pan, W.; Wang, Y.; Luo, S.; Zhao, X.; Leung, D.Y.C. Reversibility of a High-Voltage, Cl^--Regulated, Aqueous Mg Metal Battery Enabled by a Water-in-Salt Electrolyte. *ACS Energy Lett.* **2022**, *7*, 2657–2666. [CrossRef]
72. Zhou, A.; Jiang, L.; Yue, J.; Tong, Y.; Zhang, Q.; Lin, Z.; Liu, B.; Wu, C.; Suo, L.; Hu, Y.-S.; et al. Water-in-Salt Electrolyte Promotes High-Capacity $FeFe(CN)_6$ Cathode for Aqueous Al-Ion Battery. *ACS Appl. Mater. Interfaces* **2019**, *11*, 41356–41362. [CrossRef]
73. Zhang, M.; Makino, S.; Mochizuki, D.; Sugimoto, W. High-performance hybrid supercapacitors enabled by protected lithium negative electrode and "water-in-salt" electrolyte. *J. Power Sources* **2018**, *396*, 498–505. [CrossRef]
74. Bu, X.; Su, L.; Dou, Q.; Lei, S.; Yan, X. A low-cost "water-in-salt" electrolyte for a 2.3 V high-rate carbon-based supercapacitor. *J. Mater. Chem. A* **2019**, *7*, 7541–7547. [CrossRef]
75. Tribbia, M.; Pianta, N.; Brugnetti, G.; Lorenzi, R.; Ruffo, R. A new double layer super-capacitor made by free-standing activated carbon membranes and highly concentrated potassium acetate solutions. *Electrochim. Acta* **2020**, *364*, 137323. [CrossRef]
76. Zhang, M.; Li, Y.; Shen, Z. "Water-in-salt" electrolyte enhanced high voltage aqueous supercapacitor with all-pseudocapacitive metal-oxide electrodes. *J. Power Sources* **2019**, *414*, 479–485. [CrossRef]
77. Guo, J.; Ma, Y.; Zhao, K.; Wang, Y.; Yang, B.; Cui, J.; Yan, X. High-Performance and Ultra-Stable Aqueous Supercapacitors Based on a Green and Low-Cost Water-In-Salt Electrolyte. *Chemelectrochem* **2019**, *6*, 5433–5438. [CrossRef]
78. Zhang, L.; Rodríguez-Pérez, I.A.; Jiang, H.; Zhang, C.; Leonard, D.P.; Guo, Q.; Wang, W.; Han, S.; Wang, L.; Ji, X. $ZnCl_2$ "Water-in-Salt" Electrolyte Transforms the Performance of Vanadium Oxide as a Zn Battery Cathode. *Adv. Funct. Mater.* **2019**, *29*, 1902653. [CrossRef]
79. Pan, W.; Wang, Y.; Zhang, Y.; Kwok, Y.H.; Wu, M.; Zhao, X.; Leung, D.Y.C. A low-cost and dendrite-free rechargeable aluminium-ion battery with superior performance. *J. Mater. Chem. A* **2019**, *7*, 17420–17425. [CrossRef]
80. Choi, J.W.; Aurbach, D. Promise and reality of post-lithium-ion batteries with high energy densities. *Nat. Rev. Mater.* **2016**, *1*, 16013. [CrossRef]
81. Liang, Y.; Zhao, C.Z.; Yuan, H.; Chen, Y.; Zhang, W.; Huang, J.Q.; Yu, D.; Liu, Y.; Titirici, M.M.; Chueh, Y.L.; et al. A review of rechargeable batteries for portable electronic devices. *InfoMat* **2019**, *1*, 6–32. [CrossRef]
82. Köhler, U.; Antonius, C.; Bäuerlein, P. Advances in alkaline batteries. *J. Power Sources* **2004**, *127*, 45–52. [CrossRef]
83. Yoshino, A. The Birth of the Lithium-Ion Battery. *Angew. Chem. Int. Ed.* **2012**, *51*, 5798–5800. [CrossRef] [PubMed]
84. Yang, Z.; Zhang, J.; Kintner-Meyer, M.C.W.; Lu, X.; Choi, D.; Lemmon, J.P.; Liu, J. Electrochemical Energy Storage for Green Grid. *Chem. Rev.* **2011**, *111*, 3577–3613. [CrossRef] [PubMed]
85. Shin, J.; Choi, J.W. Opportunities and Reality of Aqueous Rechargeable Batteries. *Adv. Energy Mater.* **2020**, *10*, 2001386. [CrossRef]
86. Fan, X.; Liu, B.; Liu, J.; Ding, J.; Han, X.; Deng, Y.; Lv, X.; Xie, Y.; Chen, B.; Hu, W.; et al. Battery Technologies for Grid-Level Large-Scale Electrical Energy Storage. *Trans. Tianjin Univ.* **2020**, *26*, 92–103. [CrossRef]
87. Bashir, N.; Sardar, H.S.; Nasir, M.; Hassan, N.U.; Khan, H.A. Lifetime maximization of lead-acid batteries in small scale UPS and distributed generation systems. In Proceedings of the 2017 IEEE Manchester PowerTech, Manchester, UK, 18–22 June 2017. [CrossRef]
88. EV Battery Supply Chain: Trends, Risks and Opportunities in a Fast-Evolving Sector. Available online: https://store.fitchsolutions.com/all-products/ev-battery-supply-chain-trends-risks-and-opportunities-in-a-fast-evolving-sector (accessed on 29 November 2022).

89. Bhutada, G. Breaking Down the Cost of an EV Battery Cell. *Visual Capitalist.* 2022. Available online: https://www.visualcapitalist.com/breaking-down-the-cost-of-an-ev-battery-cell/ (accessed on 6 November 2022).
90. Houache, M.S.E.; Yim, C.-H.; Karkar, Z.; Abu-Lebdeh, Y. On the Current and Future Outlook of Battery Chemistries for Electric Vehicles—Mini Review. *Batteries* **2022**, *8*, 70. [CrossRef]